frontiers in Molecular Neuroscience

ORIGINAL RESEARCH
published: 23 December 2021
doi: 10.3389/fnmol.2021.757646

TALPID3/KIAA0586 Regulates Multiple Aspects of Neuromuscular Patterning During Gastrointestinal Development in Animal Models and Human

Jean Marie Delalande[1,2†], Nandor Nagy[3†], Conor J. McCann[2], Dipa Natarajan[2], Julie E. Cooper[4], Gabriela Carreno[4], David Dora[3], Alison Campbell[5], Nicole Laurent[6], Polychronis Kemos[1], Sophie Thomas[7], Caroline Alby[8], Tania Attié-Bitach[7,8,9], Stanislas Lyonnet[7,8,9], Malcolm P. Logan[10], Allan M. Goldstein[11], Megan G. Davey[12], Robert M. W. Hofstra[13‡], Nikhil Thapar[2,13] and Alan J. Burns[2,14,15]*

[1] Centre for Immunobiology, Barts and The London School of Medicine and Dentistry, Queen Mary University of London, London, United Kingdom, [2] Stem Cells and Regenerative Medicine, Birth Defects Research Centre, UCL Great Ormond Street Institute of Child Health, London, United Kingdom, [3] Department of Anatomy, Histology and Embryology, Semmelweis University, Budapest, Hungary, [4] Developmental Biology and Cancer Program, Birth Defects Research Centre, UCL Great Ormond Street Institute of Child Health, London, United Kingdom, [5] Department of Paediatric Surgery, Christchurch Hospital, Christchurch, New Zealand, [6] Génétique et Anomalies du Développement, Université de Bourgogne, Service d'Anatomie Pathologique, Dijon, France, [7] Laboratory of Embryology and Genetics of Congenital Malformations, INSERM UMR 1163 Institut Imagine, Paris, France, [8] Department of Genetics, Hôpital Necker-Enfants Malades, Assistance Publique Hôpitaux de Paris (AP-HP), Paris, France, [9] Paris Descartes, Sorbonne Paris Cité, Paris, France, [10] Randall Division of Cell and Molecular Biophysics, King's College London, London, United Kingdom, [11] Department of Pediatric Surgery, Massachusetts General Hospital, Harvard Medical School, Boston, MA, United States, [12] Division of Developmental Biology, The Roslin Institute, The University of Edinburgh, Edinburgh, United Kingdom, [13] Department of Clinical Genetics, Erasmus University Medical Center, Rotterdam, Netherlands, [14] Division of Neurogastroenterology and Motility, Department of Gastroenterology, Great Ormond Street Hospital for Children NHS Foundation Trust, London, United Kingdom, [15] Gastrointestinal Drug Discovery Unit, Takeda Pharmaceuticals International, Inc., Cambridge, MA, United States

TALPID3/KIAA0586 is an evolutionary conserved protein, which plays an essential role in protein trafficking. Its role during gastrointestinal (GI) and enteric nervous system (ENS) development has not been studied previously. Here, we analyzed chicken, mouse and human embryonic GI tissues with TALPID3 mutations. The GI tract of TALPID3 chicken embryos was shortened and malformed. Histologically, the gut smooth muscle was mispatterned and enteric neural crest cells were scattered throughout the gut wall. Analysis of the Hedgehog pathway and gut extracellular matrix provided causative reasons for these defects. Interestingly, chicken intra-species grafting experiments and a conditional knockout mouse model showed that ENS formation did not require TALPID3, but was dependent on correct environmental cues. Surprisingly, the lack of TALPID3 in enteric neural crest cells (ENCC) affected smooth muscle and epithelial development in a non-cell-autonomous manner. Analysis of human gut fetal tissues with a *KIAA0586* mutation showed strikingly similar findings compared to the animal models demonstrating conservation of TALPID3 and its necessary role in human GI tract development and patterning.

Keywords: TALPID3, KIAA0586, Sonic Hedgehog, enteric nervous system, neural crest cell, gastrointestinal tract, short-rib polydactyly syndrome, Joubert syndrome

Edited by:
Parthiv Haldipur, Seattle Children's Research Institute, United States

Reviewed by:
Meryem B. Baghdadi, Institut Curie, France
Joel C. Bornstein, The University of Melbourne, Australia

***Correspondence:**
Alan J. Burns
alan.burns@ucl.ac.uk

[†] These authors have contributed equally to this work

[‡] Deceased

Specialty section:
This article was submitted to Methods and Model Organisms, a section of the journal Frontiers in Molecular Neuroscience

Received: *12 August 2021*
Accepted: *10 November 2021*
Published: *23 December 2021*

Citation:
Delalande JM, Nagy N, McCann CJ, Natarajan D, Cooper JE, Carreno G, Dora D, Campbell A, Laurent N, Kemos P, Thomas S, Alby C, Attié-Bitach T, Lyonnet S, Logan MP, Goldstein AM, Davey MG, Hofstra RMW, Thapar N and Burns AJ (2021) TALPID3/KIAA0586 Regulates Multiple Aspects of Neuromuscular Patterning During Gastrointestinal Development in Animal Models and Human. Front. Mol. Neurosci. 14:757646. doi: 10.3389/fnmol.2021.757646

INTRODUCTION

During embryonic development, normal organogenesis depends on tightly orchestrated interactions between cells of different lineages. In the developing gastrointestinal (GI) tract, such interactions occur between ectoderm-derived neural crest cells (NCC) and the embryonic gut, which is derived from lateral mesoderm and endoderm (Zorn and Wells, 2009; Noah et al., 2011). Interactions between NCC and the developing gut subsequently determine the functional architecture of the enteric nervous system (ENS) by assuring the correct anatomical localization of the enteric neuronal plexuses and the establishment of appropriate interconnections with GI smooth muscle and the mucosa (Sasselli et al., 2012; Goldstein et al., 2013; Rao and Gershon, 2016; Nagy and Goldstein, 2017).

Amongst the numerous proteins that have been shown to be essential for correct vertebrate development is the TALPID3 protein, encoded by the *KIAA0586* gene in human (OMIM 610178). TALPID3 is a ubiquitously expressed protein. Its most recognized function is its requirement for ciliogenesis, as loss of function mutations in the *TALPID3* gene are characterized by a lack of primary cilia in model organisms (Davey et al., 2006, 2007, 2014; Bangs et al., 2011; Ben et al., 2011; Fraser and Davey, 2019; Yan et al., 2020). It has been shown that the TALPID3 protein has an evolutionary conserved intracellular localization at the centrosome, which plays a critical role in ciliogenesis and coordination of ciliary protein trafficking, in particular through functional interactions with Rab8 and Mib1 (Yin et al., 2009; Ben et al., 2011; Mahjoub, 2013; Sung and Leroux, 2013; Villumsen et al., 2013; Kobayashi et al., 2014; Wu et al., 2014; May-Simera et al., 2016; Wang et al., 2016; Li et al., 2017; Naharros et al., 2018). TALPID3 has also been shown to be important for centriole duplication (*via* direct binding to CEP120), as well as centriolar satellite dispersal, centrosome length and orientation, which regulates overall tissue polarity (Wu et al., 2014; Stephen et al., 2015; Tsai et al., 2019). In human, the phenotypic spectrum of *KIAA0586* mutations (the human ortholog of chicken *talpid*^{3}) expands from embryonic lethal ciliopathies to pediatric ciliopathy symptoms including Joubert Syndrome (JBTS) (Akawi et al., 2015; Alby et al., 2015, 2016; Bachmann-Gagescu et al., 2015; Malicdan et al., 2015; Roosing et al., 2015; Stephen et al., 2015). A conditional deletion of *talpid*^{3} in the central nervous system of a mouse model recapitulates the cerebellar phenotype seen in JBTS (Bashford and Subramanian, 2019).

The severe developmental defects caused by the lack of TALPID3 can be linked to the disruption of key developmental signaling pathways, with the strongest association shown to be with the Hedgehog (Hh) pathway (Davey et al., 2006, 2007, 2014; Ben et al., 2011; Ingham, 2016; Matsubara et al., 2016; Fraser and Davey, 2019). Three Hh gene homologs have been described in vertebrates: *Sonic Hedgehog* (*shh*), *Indian Hedgehog* (*ihh*), and *Desert Hedgehog* (*dhh*) (Pathi et al., 2001; Ingham, 2016). At the sub-cellular level, following the binding of Hedgehog ligands to the Patched receptor (PTCH1), the *trans*-membrane transducer Smoothened (SMO) is transported to the primary cilium by anterograde trafficking. Subsequently, GLI proteins located within the cilium tip are processed into activator (GLIA) or repressor (GLIR) isoforms, which are then released in the cytoplasm. The processing of GLI proteins through the cilium establishes the ratio of GLIA to GLIR proteins, which in turn act as transcriptional effectors to control downstream SHH target genes (Kim et al., 2009; Pan et al., 2009; Sasai and Briscoe, 2012; Briscoe and Therond, 2013; Ramsbottom and Pownall, 2016). TALPID3 has been shown to interact and colocalize with the PKA regulatory subunit PKARIIβ at the centrosome. This interaction leads to the phosphorylation of GLI2 and GLI3 and directly links TALPID3 to a functional step in the Hh pathway (Li et al., 2017).

Many studies have demonstrated the central role of the Hh pathway in gut development, physiology and cancer [reviewed in Fukuda and Yasugi (2002); van den Brink (2007), and Merchant (2012)]. Normal gut development has both common and separate requirements for SHH and IHH. In mouse models, mutations in *shh* or *ihh* result in reduced smooth muscle mass, gut malrotation and annular pancreas (Ramalho-Santos et al., 2000). In addition, *shh* mutants exhibit specific defects such as intestinal transformation of the stomach, duodenal stenosis, increased enteric neurons, abnormally distributed ganglia and imperforate anus. On the other hand, *ihh* mutants show reduced epithelial stem cell proliferation and differentiation rate, as well as aganglionic colon (Ramalho-Santos et al., 2000). Interestingly, mutant mice lacking hedgehog-binding protein growth arrest–specific gene 1 (Gas1) or its intracellular messenger Gnaz, have a shortened digestive tract, reduced smooth muscle mass, increased number of enteric neurons and miss-patterned ENS (Kang et al., 2007; Biau et al., 2013). This phenotype has been attributed to a combination of reduced Hh signaling and increased Ret tyrosine kinase signaling (Biau et al., 2013). The Ret tyrosine kinase is essential for ENS development (Natarajan et al., 2002).

Here, we examined the GI tracts of *talpid*^{3} chicken and human fetal gut tissues bearing a homozygous null mutation in *KIAA0586*. We found remarkably similar phenotypes and comparable defects in gut tissues (Schock et al., 2016). We also investigated the role of *TALPID3* in early formation of the ENS, using chicken chimeras and a *talpid*^{3} conditional knock out mouse. We demonstrate that *TALPID3* is not required cell autonomously for ENCC migration and early ENS patterning. Rather, our results demonstrate that *TALPID3* is essential for normal spatial differentiation of smooth muscle and proper expression of ECM components. Our study also reveals that growth and development of both mucosa and smooth muscle are regulated by the ENS *via TALPID3*-mediated signaling.

RESULTS

talpid^3 Chicken Embryos Have Multiple Anatomical Defects Including Gastrointestinal Defects

talpid^3 is a naturally occurring chicken mutant. The *talpid*^{3} mutation is recessive and leads to leaky blood vessels among

other defects. This is causing very high embryonic mortality as reported in both chicken and mouse *Talpid*^{3} models (Davey et al., 2006; Ben et al., 2011). Although limbs and organ defects have been reported in *talpid*^{3} chicken embryos, there has been a lack of detailed analysis of the GI defects in these mutants. As previously described, Buxton et al. (2004) E10.5 *talpid*^{3} chick embryos were smaller than controls, showed generalized edema and displayed a wide range of congenital abnormalities including short ribs, polydactylous paddle shaped limbs, organ defects (lung hypoplasia, liver fibrosis, and cholestasis) and craniofacial abnormalities (hypotelorism, reduction and anterior displacement of the frontonasal process) (**Figure 1A**). At E10.5, the GI tract of *talpid*^{3} chick embryos was significantly reduced in length compared to controls (**Figure 1B**). As previously described, no left right asymmetry or rotation defect was observed in the stomach of *talpid*^{3} chick embryos (Stephen et al., 2014). Transverse sections at the level of the neck showed abnormal connection (fistula) between the esophagus and the trachea or a total absence or narrowing (atresia) of either of the structures (**Figures 1G,O**). Additionally, *talpid*^{3} embryos had an open hindgut (**Figure 1B** – inset-, J,R). Lastly, gut epithelium thickness varied between controls and mutants, as shown in **Figures 1M,Q** insets.

Severe Smooth Muscle and Enteric Nervous System Patterning Defects in *talpid*^{3} Chicken Gastrointestinal Tract

To gain further insight into the GI defects of *talpid*^{3} embryos we performed immunohistochemistry using molecular markers to highlight the neuromuscular organization of the GI tract in controls and *talpid*^{3} mutants. In E8.5 controls, smooth muscle actin (SMA) immunostaining revealed a compact ring of immunopositive cells, corresponding to the presumptive circular muscle layers, encircling the gut epithelium (**Figures 1C–F**). Notably, this muscular ring was located in the outer mesenchyme, with a distinct separation between the muscle and the gut epithelium (**Figures 1C–F**, double arrows). In *talpid*^{3} gut, despite the presence of SMA staining surrounding blood vessels, SMA positive cells were discontinuous or absent around the esophagus (**Figure 1G**). In the stomach and the intestine, the compact muscular ring seen in controls was replaced by diffuse staining that extended across the entire gut mesenchyme, with SMA positive cells abutting the gut epithelium (**Figures 1H,I**, arrowheads). In the colorectum, the circular muscular pattern was disrupted by the open hindgut phenotype (**Figure 1J**). In E8.5 controls, TuJ-1 immunostaining revealed ENCC-derived neurons arranged in characteristic plexuses (**Figures 1K–N**). In the esophagus and the stomach, the presumptive ENS was organized in a single plexus located in the outermost mesenchyme (**Figures 1K,L**, double arrows). In the intestine and colorectum, ENCC were organized in two plexuses: the myenteric plexus (MYP) and the submucosal plexus (SMP) (**Figures 1M,N**). The nerve of Remak (Rem), an avian specific nerve derived from sacral ENCC, was also positively labeled (**Figure 1N**). In E8.5 TALPID3 embryos, ENCC were present throughout the intestine (**Figure 1Q**) and colorectum, although well-defined plexuses were not apparent in the distal gut due to the open hindgut phenotype (**Figure 1R**). Although ENCC were observed alongside the esophagus at E6.5 (data not shown), they were not found around the esophagus at E8.5 and did not form a plexus (**Figure 1O**). At this stage, ENCC were present in the stomach and intestine regions, but they failed to organize in plexuses and were scattered throughout the gut wall (**Figures 1P,Q**). In the colorectum, the nerve of Remak was also smaller in diameter and/or comprised several bundles (**Figures 1Q,R**). The presence of ENCC in distal parts of the GI tract demonstrated that TALPID3 is not required for ENCC migration *per se*. knowing the role of TALPID3 in ciliogenesis, we looked at the presence of primary cilia on migrating ENCC (**Supplementary Figure 1**). In chicken neural tube cultured *in vitro*, primary cilia were readily evident on the neural tube cells. However, we failed to observe them on migrating vagal ENCC, either anatomically by SEM or molecularly using immunofluorescence (**Supplementary Figures 1A–D**). *In vivo*, despite primary cilia being readily detected in E6.5 chicken gut sections, only 11% of HuC$^+$ ENCC showed a detectable primary cilium (**Supplementary Figures 1E,F**). Overall, these results showed regions such as the esophagus being devoid of both ENS and smooth muscle in *talpid*^{3} mutants, whereas regions such as the ventral stomach and the intestine showed scattered ENS and extended regions of smooth muscle differentiation across the mesenchyme.

Hh Signaling Is Disrupted in *talpid*^{3} Gastrointestinal Tract

Due to the well-established functional connection between *TALPID3* and Hh signaling, we investigated changes in this pathway in control and *talpid*^{3} mutants using *in situ* hybridization. *In situ* analysis of *shh* expression in the GI tract of E6.5 control and *talpid*^{3} embryos revealed transcripts in the gut epithelium of both type of tissues, demonstrating expression of the *shh* gene in the *talpid*^{3} mutants (**Figures 5A–H**). Expression of SHH was confirmed in the endoderm of the intestine using an anti-SHH antibody (**Supplementary Figure 2**). To visualize the readout of Hh signaling in the gut wall, mRNA expression of the Hh receptor *PTCH1* was used. In E6.5 control embryos, the pattern of expression of *PTCH1* was composed of one or two concentric gradients surrounding the epithelium (**Figures 5I–L**). In the esophagus, the ventral part of the stomach and the intestine, two concentric gradients were present; the first was located adjacent to the epithelium in the sub-epithelial mesenchyme, and the second more distally located in the outer mesenchyme (**Figures 5I–K**). In the dorsal part of the stomach and the colorectum a single sub-epithelial gradient was present (**Figures 5J,L**). Strikingly, the discrete characteristic gradients of *PTCH1* expression were absent in the GI tract of *talpid*^{3} mutants. Instead a diffuse homogenous expression was observed throughout the gut wall and the epithelium. The same diffuse *PTCH1* pattern was observed at all levels of the GI tract (**Figures 5M–P**). Together these

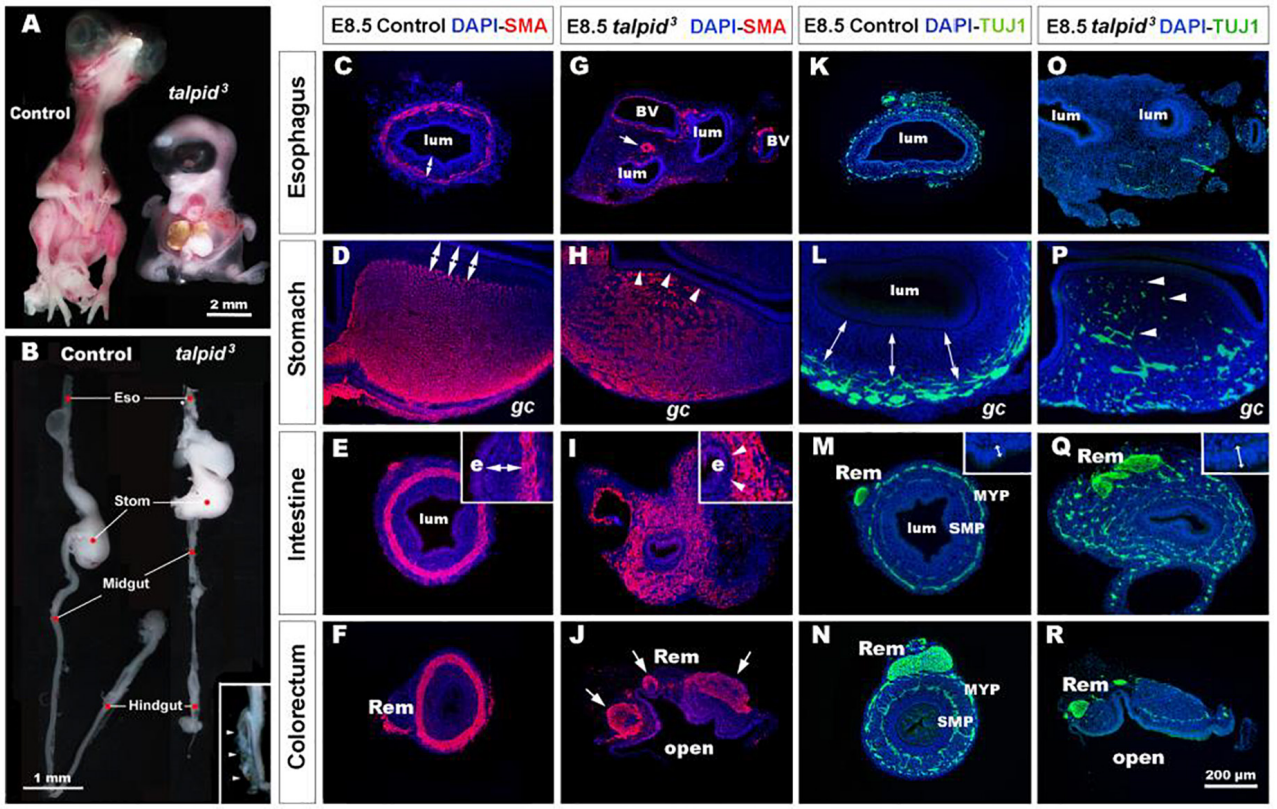

FIGURE 1 | *talpid*^{3} embryos have multiple gastrointestinal defects, including disruption of the neuromuscular patterning of the digestive tract. **(A)** Phenotype of control (left) and *talpid*^{3} (right) embryos at E10.5. *talpid*^{3} mutant embryos have paddle-shaped limbs and hypotelorism. **(B)** Anatomical features of the GI tract along the rostro-caudal axis (esophagus, stomach, intestine, cecum, and colorectum) of E10.5 control embryos (left). In stage-matched *talpid*^{3} embryos (right), all gut regions are apparent, but the esophagus and trachea are malformed, midgut and hindgut are reduced in length, and the terminal hindgut is open. (Inset in **B**) High magnification of an open hindgut (arrowheads). **(C–J)** Expression of smooth muscle actin (SMA) at E8.5 in controls **(C–F)** and **(G–J)** *talpid*^{3} embryos. **(C–F)** In controls, SMA is expressed in the presumptive circular muscle layer in the outer mesenchyme, distant from the epithelium (**C–E**, double arrows). **(G)** In E8.5 *talpid*^{3} embryos, the SMA staining of the esophagus is discontinuous unlike the SMA surrounding blood vessels (arrows). **(H,I)** SMA staining in the stomach and midgut of mutants is widespread throughout the gut wall, with staining extending adjacent to the epithelium (e) and the serosa (s) (**H,I**, arrowheads). **(J)** SMA staining in the colorectum shows disrupted muscle and open hindgut. **(K–R)** Expression of TuJ-1 labeled enteric neural crest at E8.5 in **(K–N)** controls and **(O–R)** *talpid*^{3} embryos. **(K–N)** In E8.5 controls, TuJ-1 staining shows enteric neural crest organized in one **(K)** or two plexuses **(L–N)** clearly separated from the mucosa (double arrows). **(M,N)** The Remak nerve is a single bundle of fibers. **(O–R)** In *talpid*^{3} E8.5 embryos, TuJ-1 staining shows enteric neural crest cells are absent **(O)** or scattered throughout the mesenchyme (**P–R**, arrowhead). The Remak nerve is divided in several bundles **(Q,R)**. Epithelium thickness varies between control and mutant intestine (**M,Q** – inset). e, endoderm; *gc*, greater curvature of the stomach; lum, lumen; m, mucosa; Rem, nerve of Remak; MYP, myenteric plexus; SMP, submucosal plexus; BV, blood vessels. Same scale bar in **(C–R)**.

results showed that, despite epithelial expression of SHH in *talpid*^{3} mutants, the precise integration of the signal in the surrounding mesenchyme was lost, as shown by the aberrant *PTCH1* expression.

Defective Expression of Extracellular Matrix Components in *talpid*^{3} Gut Mesenchyme Leads to the Disappearance of Neural Crest Cells Repellent Cues

In search of a mechanistic explanation for the lack of ENS plexus formation in *talpid*^{3} mutants, we analyzed expression of components of the gut ECM known to influence neuronal behavior (Tennyson et al., 1990; Siebert et al., 2014; Nagy et al., 2016). First, we used the CS-56 antibody, which stains the glycosaminoglycan portion of native chondroitin sulfate proteoglycans (CSPG). CSPG are ECM components regulated by Hh signaling (Nagy et al., 2016). In E6.5 control tissues, CS-56 staining comprised two concentric gradients: the first immediately adjacent to the gut epithelium (sub-epithelial mesenchyme) and the second located in the outer gut wall (outer mesenchyme) (**Figure 4A**). This expression pattern was very similar to *PTCH1* as described above. In E6.5 *talpid*^{3} gut tissues, CS-56 expression was absent from the outer mesenchyme, with only cells adjacent to the epithelium staining positive (**Figure 4F**). Additionally, we examined the expression of Collagen 9 (Coll9), a ECM component expressed in the developing gut, which has been specifically shown to elicit avoidance behavior by neural crest cells *in vitro*

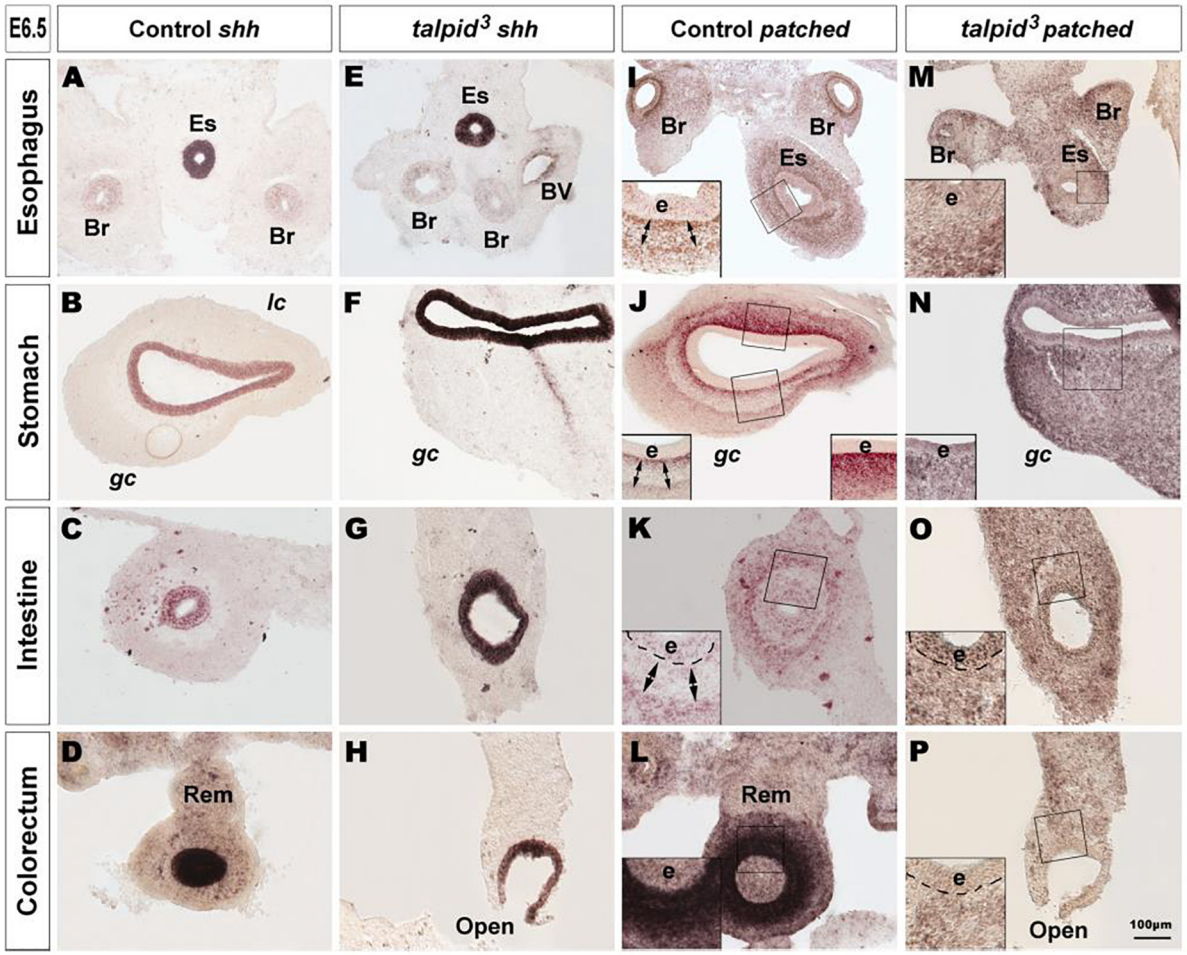

FIGURE 2 | Hh signaling is disrupted in the GI tract of *talpid*^{3} mutants. **(A–P)** *In situ* hybridization for *shh* **(A–H)** and *patched* **(I–P)** in E6.5 control **(A–D,I–L)** and E6.5 *talpid*^{3} mutant **(E–H,M–P)** transverse sections. **(A–H)** In both controls and *talpid*^{3}, *shh* is expressed in the endoderm in all gut regions. **(I–L)** *Patched in situ* in controls shows a discrete pattern of expression with one (**J–L** + insets) or two (**I–K** + Insets) concentric gradients. (**M–P** + insets) In *talpid*^{3} sections the *patched* gradient is replaced by uniform levels of expression. Es, esophagus; Br, bronchus; Rem, nerve of Remak; e, endoderm; *lc*, lesser curvature; *gc*, greater curvature of the stomach. Same scale bar in **(A–P)**.

(Ring et al., 1996; Nagy et al., 2016). Consistent with the CS-56 staining, Coll9 pattern of expression was also composed of two concentric areas, one within the sub-epithelial mesenchyme and one in the outer mesenchyme (**Figures 4B,D**). Interestingly, the Coll9 expression pattern appeared to define exclusion zones for the migrating ENCC, which were only present outside Coll9 positive areas, as shown by N-cadherin (NCadh) staining (**Figures 4B,C**; double arrows). As seen with CS-56, there was no Coll9 expression in the outer mesenchyme of E6.5 *talpid*^{3} gut samples and only the sub-epithelial mesenchyme was stained (**Figures 4G,H**). Interestingly, and in correlation with the lack of outer mesenchyme Coll9 expression, NCadh-positive ENCC were scattered throughout the gut mesenchyme, with some cells located adjacent to the epithelium (**Figures 4G,H**; arrowheads in inset). We also investigated the expression of Coll9 respective to smooth muscle differentiation. We found that SMA and Coll9 have distinct, yet partially overlapping, patterns of expression in control tissues (**Figures 4D,E**). In E6.5 control esophagus, the distal gradient of Coll9 corresponded with the inner boundary of the smooth muscle ring (**Figure 4D**). In the stomach, Coll9 and SMA were mostly mutually exclusive apart from a subdomain in the ventral region where both were co-expressed (**Figure 4E**). In E6.5 *talpid*^{3} esophagus, both the Coll9 distal gradient and the SMA ring were absent (**Figure 4I**). In the *talpid*^{3} stomach, most of the Coll9 expression domain was absent compared to control, while the SMA-positive domain was extended (**Figure 4J**). These results show that expression of CSPG in the gut mesenchyme is regulated by *talpid*^{3} (likely indirectly via the dysregulation of the Hedgehog pathway), as its absence led to significant loss in expression of these ECM components. Moreover, the changes in ECM components expression were concurrent with mislocalization of migrating ENCC.

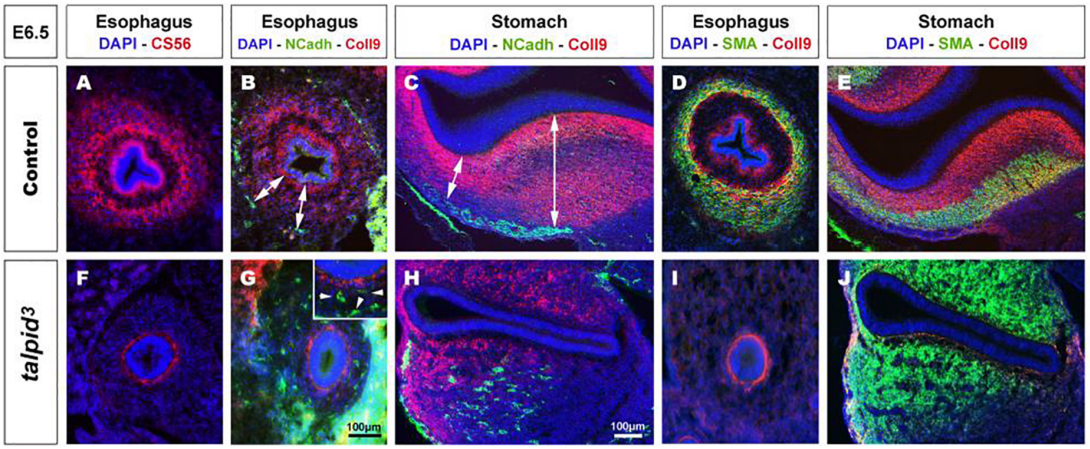

FIGURE 3 | Expression of chondroitin sulfate proteoglycans (CSPG) is altered in *talpid*^{3} gut mesenchyme, causing the disappearance of ENCC repellent cues. **(A–J)** Immunofluorescent staining of esophagus and stomach with CSPG pan marker CS-56 and Coll9, in control **(A–E)** and *talpid*^{3} chicken mutant **(F–J)** at E6.5, **(B,C,G,H)** co-stained with N-Cadherin and **(D,E,I,J)** smooth muscle actin (SMA). **(A,B,D)** In the esophagus, the pattern of two concentric circles of CSPG expression is lost in **(F,G,I)** *talpid*^{3} mutant (**G**-inset, arrowheads) coinciding with scattered ENCC. **(C)** In control stomach, Coll9 expression is widespread and excludes the ENS myenteric plexus whereas in (**H**, double arrows) *talpid*^{3} mutant expression is altered and loss of expression coincides with scattered ENCC. **(D,E)** In control, SMA expression in partially overlapping with Coll9 (yellow merge). **(I,J)** in *talpid*^{3} mutants, Coll9 expression is altered and SMA is either lost **(I)** or extends to ectopic sub-epithelial domains **(J)**. Same scale bar in **(A–J)**.

Transplantation of Wild Type Enteric Neural Crest Cells Does Not Rescue the Formation of Enteric Nervous System Plexuses in a *talpid*^{3} Gut

To investigate the role of *TALPID3* in ENS plexus formation, we attempted to rescue normal ENS patterning in *talpid*^{3} mutants by grafting wild type neural tubes, including neural crest, into *talpid*^{3} host embryos (**Figure 3**). GFP chicken tissues were used as donors for the transplants, so that vagal ENCC had a functional *TALPID3* protein and could also be traced in the chimeric embryos using GFP expression. When compared to GFP > wild type transplanted controls (**Figures 3A–D**) or stage matched *talpid*^{3} embryos (**Figures 3I–L**), transplanted GFP + ENCC behaved similarly to ENCC of *talpid*^{3} embryos and were unable to rescue ENS patterning (**Figures 3E–H**). At the level of the esophagus, instead of surrounding the esophagus in a presumptive circular plexus, as seen in controls (**Figure 3A**), transplanted GFP + ENCC clustered in the dorsal region (**Figure 3E**), in a pattern similar to that seen in *talpid*^{3} embryos (**Figure 3I**). In the stomach and intestine, transplanted GFP + ENCC migrated similar distances along the GI tract as observed in *talpid*^{3} embryos but were scattered throughout the mesenchyme (**Figures 3F,G,J** + inset G) and not arranged in plexuses, as seen in controls (**Figures 3B–D** + inset C). Epithelium and smooth muscle thickness (stained with DAPI and Phalloidin, respectively) in intestine and stomach sections were measured in stage matched GFP > wild type and GFP > *talpid*^{3} chimera, as well as *talpid*^{3} mutants. Measurements from GFP > *talpid*^{3} chimeric tissues and *talpid*^{3} mutant were both statistically ($^{***}p < 0.001$) different from the controls (**Supplementary Figure 3**). The non-parametric Spearman's Rho test was used to measure the correlation between GFP > wild type and GFP > *talpid*^{3} chimera, and *talpid*^{3} mutants measurements. The correlation between GFP > wild type and GFP > *talpid*^{3} transplants was 0.670, whereas the correlation between the GFP > wild type transplant and the *talpid*^{3} mutant was 0.715. Importantly, the correlation between the GFP > *talpid*^{3} and the *talpid*^{3} mutant was 0.942, an extremely high score. The fact that measurements from chimera and mutant clustered together and were statistically different from the control supported histological findings of a lack of rescue. Overall, wild type transplanted vagal ENCC did not rescue ENS plexus formation or the smooth muscle phenotype in a *talpid*^{3} environment.

Lack of TALPID3 in Enteric Neural Crest Cells Does Not Affect Gross Enteric Nervous System Morphology but Affects Smooth Muscle and Mucosa Development in a Non-cell-autonomous Manner

To further assess the role of TALPID3 during ENS development and to test its cell autonomous requirement in ENCC, we performed the converse experiment to that described above, by grafting *talpid*^{3} vagal ENCC into GFP-expressing chick embryos. In the resulting chimeric embryos, the transplanted ENCC were devoid of functional TALPID3 protein and were identified by lack of GFP expression (GFP^{-ve}; **Figure 2** inset). Due to the extremely high mortality of this type of chimera, only one specimen survived to E7.5 for the gut tissues to be analyzed. Surprisingly, transplanted vagal

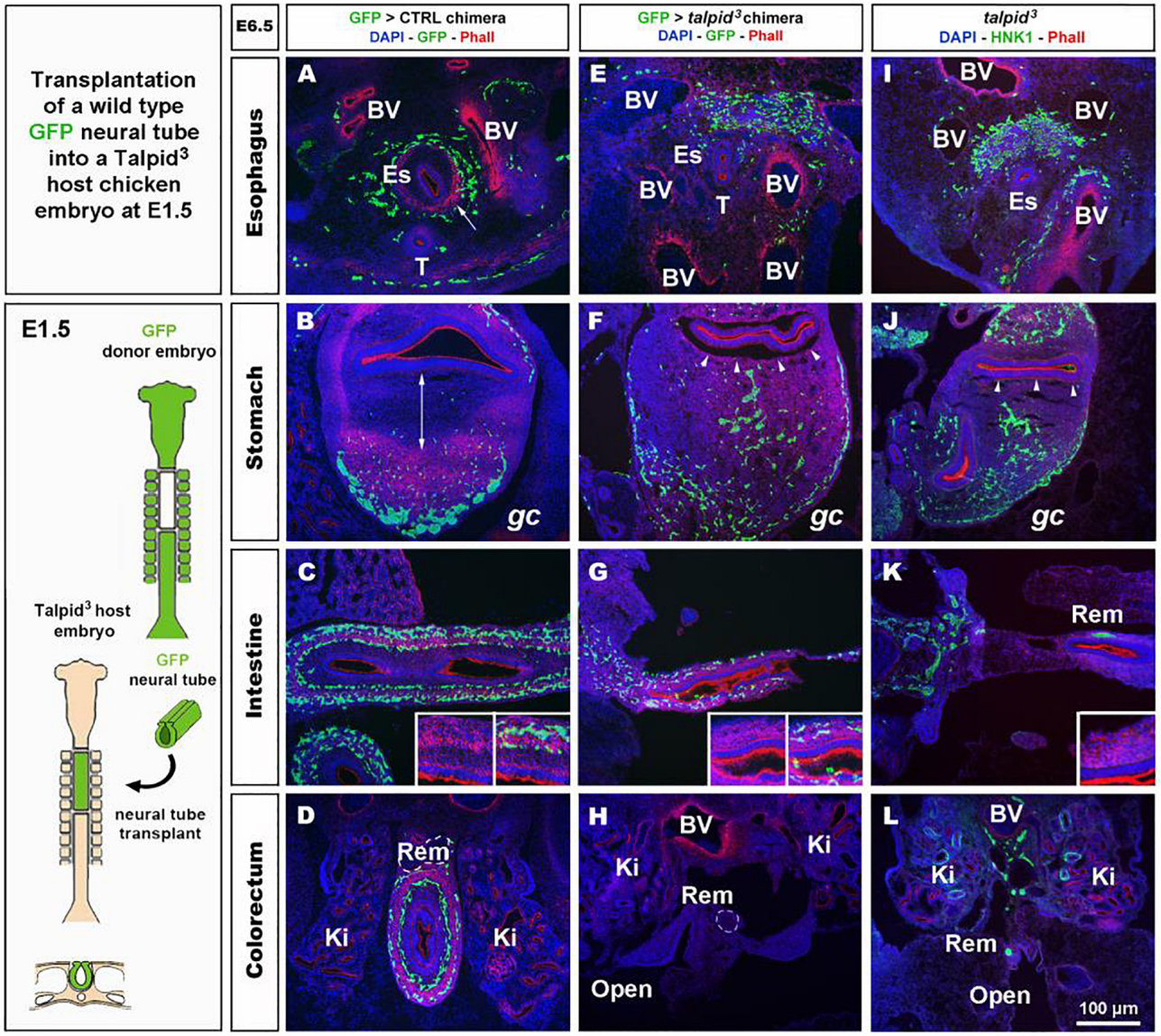

FIGURE 4 | GFP > *talpid*^{3} chimeric embryos show ENS and smooth muscle patterning defects similar to stage matched *talpid*^{3} embryos. **(A–L)** E6.5 chimeric embryos after wild type GFP neural tube transplantation in **(A–D)** GFP > control and **(E–H)** GFP > *talpid*^{3} hosts, compared to **(I–L)** E6.5 *talpid*^{3} embryos. **(A–L)** Immunofluorescent staining for GFP and Phalloidin in **(A–H)** chimeric embryos and **(I–L)** HNK-1 and phalloidin in *talpid*^{3} embryos. (**E–G** + inset) GFP > *talpid*^{3} chimeric embryos have scattered ENCC distribution similar to TALPID3 embryos. **(A–D)** Phalloidin staining shows smooth muscle patterning in control chimera (arrow, double arrow, insets). **(E–H)** Phalloidin staining shows a lack of smooth muscle patterning in the GFP > *talpid*^{3} chimera, similar to the staining found in *talpid*^{3} embryos (**I–L**; arrowheads, inset). BV, blood vessels; Ki, kidneys; Rem, nerve of Remak; Es, esophagus; T, trachea; *gc*, greater curvature of the stomach. Same scale bar in **(A–L)**.

talpid^3 ENCC migrated throughout the GI tract and patterned normally into the characteristic MYP and SMP of the ENS, as shown by HNK1 and GFP staining at E7.5 (**Figures 2A–H**). Importantly, *talpid*^{3}ENCC colonized the entire length of the GI tract and were found in the colorectal region (**Figure 2H** + inset). Here, vagal GFP^{-ve} ENCC (red) were present alongside GFP$^+$ (yellow) ENCC (**Figure 5H** left inset) that were likely sacral ENCC entering the gut prematurely (Burns and Le Douarin, 2001). In contrast to the ENS, which was grossly normal in the chimeric embryo, there were obvious defects in smooth muscle differentiation as revealed by SMA staining: instead of the characteristic SMA$^+$ ring of differentiating smooth muscle cells seen at E7.5 in control chimeras (**Figures 2I–P** + insets J,N), there was thickened and diffuse SMA staining in regions of the esophagus and the stomach, suggesting impaired differentiation (**Figures 2I,J,M,N** double arrows + insets J,N; **Figure 6H**). The characteristic SMA$^+$ ring of cells

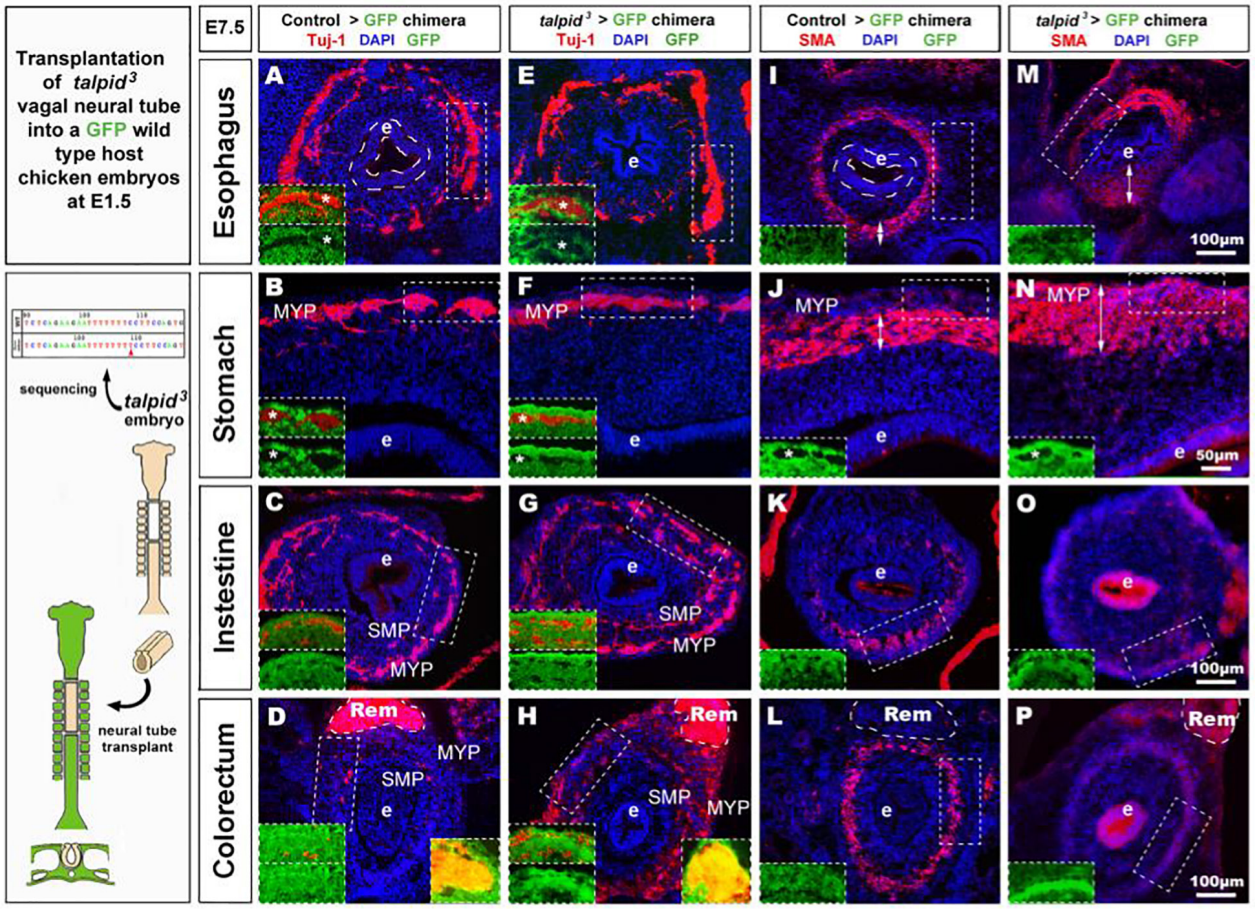

FIGURE 5 | *talpid*^{3} > GFP chimeric embryos have grossly normal ENS but smooth muscle and epithelium defects. **(A–P)** E7.5 chimeric embryos after neural tube transplantation in **(A–D,I,J)** control > GFP and **(B–H,M–P)** *talpid*^{3} > GFP. **(A–P)** Immunofluorescent staining for a TUJ-1+ and GFP [inset] in **(A–H)** and SMA and GFP [inset] in **(I–P)**. Panels **(A–H)** normal ENS patterning is observed in both control > GFP and *talpid*^{3} > GFP. (**D,H** insets) show the presence of (red) vagal TUJ-1+/GFP- ENCC (marked with asterisks *), as well as (yellow) TUJ-1+/GFP+ sacral ENCC in the Remak nerve. **(E–H)** TUJ-1 staining shows grossly normal ENS in *talpid*^{3} > GFP chimera with a more mature/developed appearance of the ENS in the intestine and colon compared to the control chimera. **(I–L)** Well-defined circular SMA staining in control chimera. **(M–P)** Diffuse SMA expression and/or extended SMA domain (double headed arrows) in *talpid*^{3} > GFP chimera. **(O)** SMA staining is almost absent in intestine of *talpid*^{3} > GFP chimera. **(P)** Diffuse, yet circular SMA staining present in colorectum of *talpid*^{3} > GFP chimera. **(A,E,I,M)** The endoderm of *talpid*^{3} > GFP chimera is significantly thinner than controls at the level of the esophagus. e, endoderm; Rem, nerve of Remak; MYP, myenteric plexus; SMP, submucosal plexus. Same scale bar in **(A–P)**.

was also missing in the intestine of the chimeric embryo (**Figure 2O**). Normal SMA staining was observed in some areas around the esophagus and within the colorectum, which coincided with the presence of normal vagal ENCC from the region adjacent to the graft and wild type sacral ENCC, respectively (**Figure 2H** inset). Additionally, the architecture of the mucosa was disrupted in the chimeric embryo, with the esophageal epithelium consisting of a thin folded monolayer, unlike controls where a thickened circular epithelium was present (**Figures 2A,E,I,M** doted lines). Using DAPI, SMA, and TuJ-1 staining, epithelial cells, smooth muscle cells and enteric neurons were counted on stomach sections ($n = 3$ sections minimum, as shown in **Figures 2B,F,J,N**). Numbers were combined with equivalent murine data for chicken/mouse cross-species statistical analysis of chimeric animals where *Talpid3* was knocked down in ENCC, as described below (**Figure 6H**).

Because only one *talpid*^{3} > GFP chicken chimera could be analyzed (due to extremely high mortality) we wished to confirm the chicken results using an alternative approach. For this, we engineered a conditional knock out of the *Talpid3* gene in a mouse model by crossing a *Wnt1:Cre* line (Danielian et al., 1998), with a floxed *Talpid3* knock-out line. Resultant *Wnt1:Cre;Talpid3* $^{flox/flox}$ embryos, which do not express TALPID3 in NCCs, were often embryonic lethal or died at P0, due to presumptive respiratory problems, as their lungs failed to fill with air (**Supplementary Figure 4**). P0 pups showed a craniofacial phenotype characteristic of hypoplastic neural crest derivatives (**Supplementary Figures 3D,F**). In mutants, the GI tract morphology was grossly normal

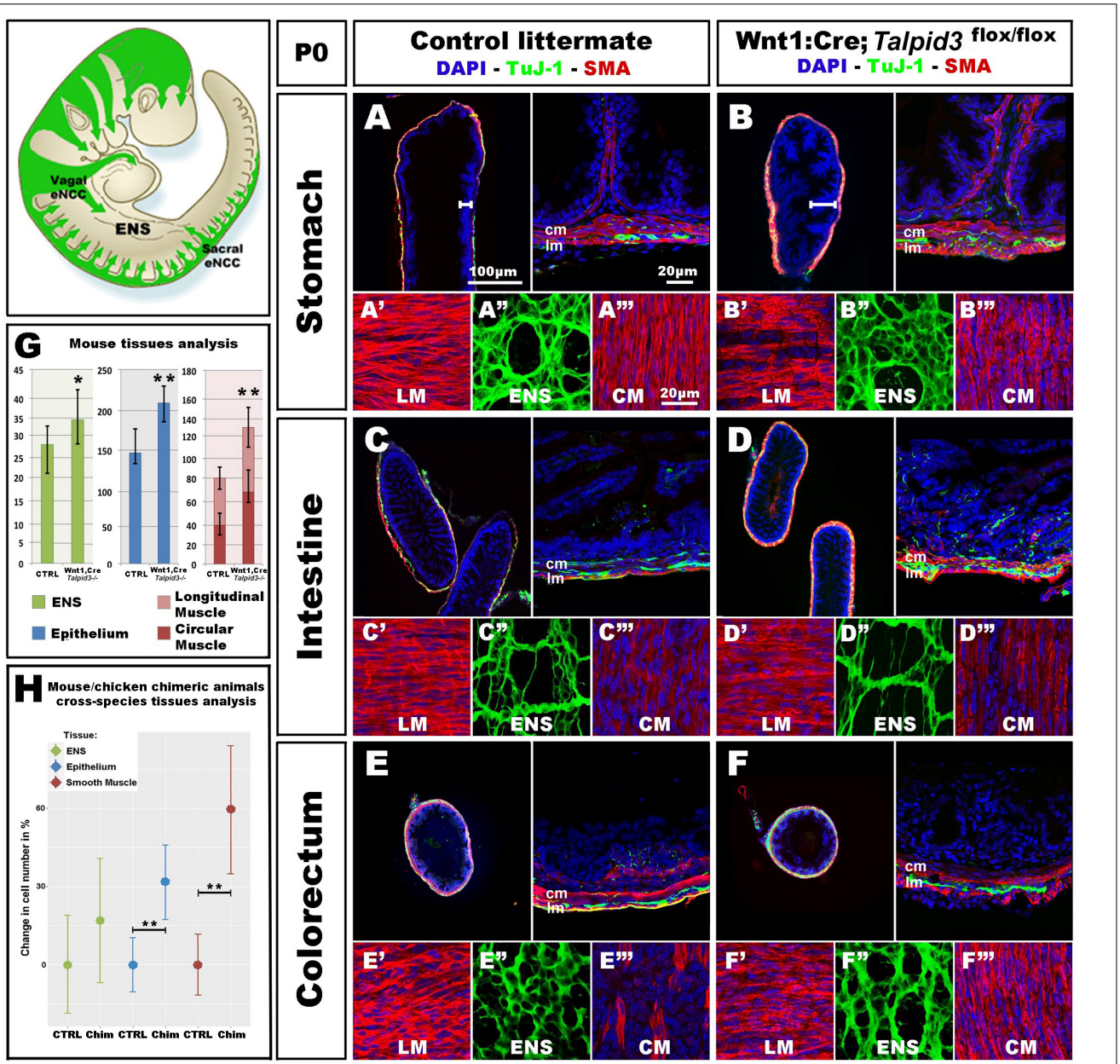

FIGURE 6 | *Wnt1:Cre;Talpid3*$^{flox/flox}$ mice show grossly normal ENS but smooth muscle and epithelium defects. **(A–F)** Immunofluorescent staining for TuJ-1 and SMA at the level of **(A,B)** the stomach, **(C,D)** intestine and **(E,F)** colorectum in control littermate and *Wnt1:Cre;Talpid3*$^{flox/flox}$ P0 pups, respectively. **(A′–A‴,B′–B‴,C′–C‴)** confocal projections at the level of the longitudinal muscle (LM), enteric nervous system (ENS) and circular muscle (CM), respectively. **(G)** Bar graph shows cell counts for ENS, LM, CM and total smooth muscle, as well as epithelium in control littermate versus *Wnt1:Cre;Talpid3*$^{flox/flox}$. In the stomach, the ENS (green) showed a statistically significant (*$p = 0.045$) increase of 29% in the number of ENCC in the mutant, compared to control. Epithelium (blue) showed a statistically significant (**$p = 0.009$) increase of 39% in the mutant, compared to control. Muscle layers (red) showed a highly statistically significant (**$p = 0.002$) increase of 67% in mutant tissue sections compared to control, with 80% increase in the longitudinal muscle (**$p = 0.002$) and 55% increase in the circular muscle (**$p = 0.018$). Difference in epithelium thickness is highlighted in **(A,B)** by white bars. **(H)** Scatter plot shows mouse/chicken cross-species cell counts for ENS, epithelium and smooth muscle in stomach of controls and chimeric animals. Epithelium (blue) showed a statistically significant (**$p = 0.009$) increase of 39% in the mutant, compared to control. Muscle layers (red) showed a highly statistically significant (**$p = 0.002$) increase of 67% in mutant tissue sections compared to control. ctrl, control; chim, chimera; cm, circular muscle; lm, longitudinal muscle. Same scale bars in **(A–A‴–F–F‴)**.

compared to control littermates (**Supplementary Figures 4B,E**). As seen in the chicken model, *Talpid3* ENCC colonized the entire length of the gut and formed an apparently normal ENS all along the GI tract (**Figures 6A–F,A″–F″**). Although the ENS was grossly normal, quantitative analysis of the ENS in the stomach region showed a statistically significant ($p = 0.045$) increase of 29% in the number of ENCC in the mutants ($n = 8$ sections) (**Figure 6G**). Of

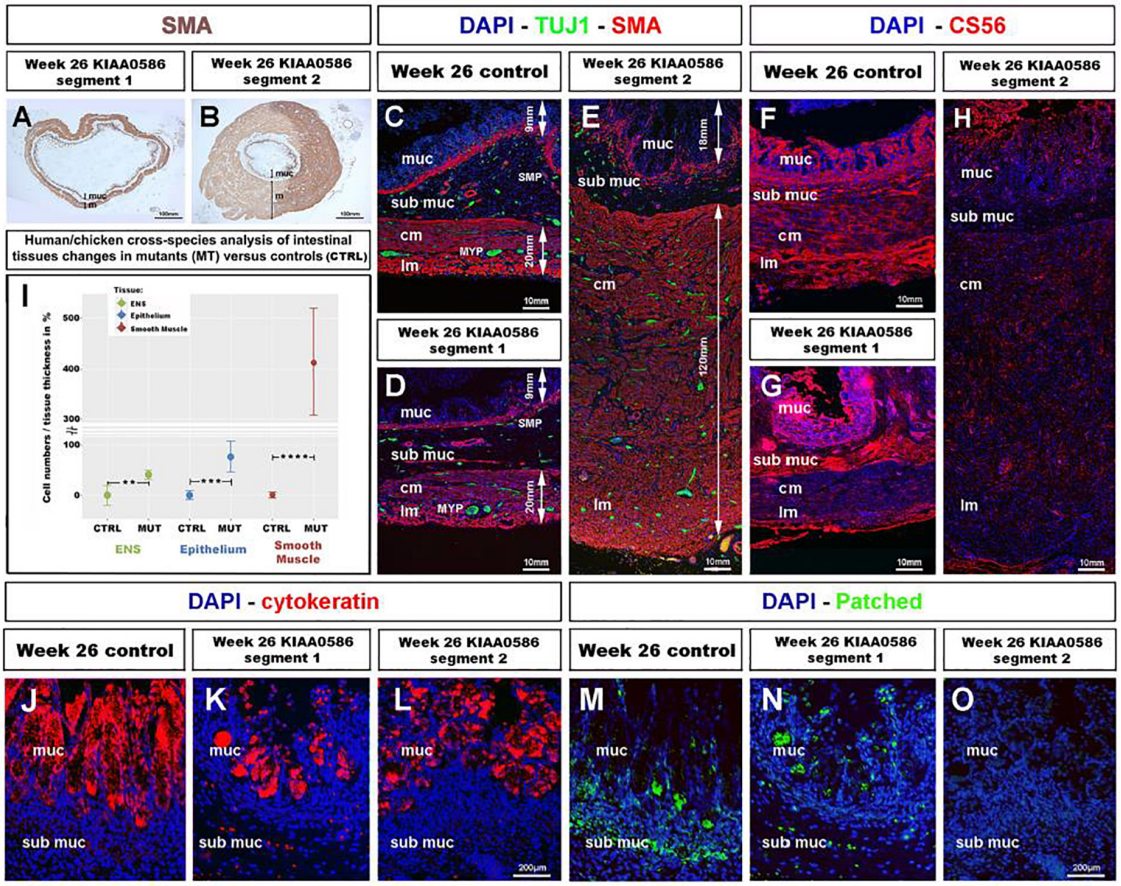

FIGURE 7 | Fetal GI tissues from a 26 weeks human fetus bearing a *KIAA0586* mutation show one gut segment with scattered ENS, mucosa and smooth muscle overgrowth, as well as CS56, Cytokeratin and Patched expression defects. **(A,B)** Low magnification gut sections of a 26 weeks fetus with a *KIAA0596* mutation. SMA immuno-staining reveals grossly normal smooth muscle layers in **(A)** "segment 1" of the intestine and extensive smooth muscle and mucosa overgrowth in **(B)** "segment 2". **(C–E)** Immunofluorescence staining for DAPI (nucleus), TuJ-1 (ENS), and SMA (Smooth Muscle) on intestine sections. **(C)** 26 weeks control intestine with normal ENS patterning and longitudinal and circular smooth muscle layers. Panels **(D,E)** staining in the *KIAA0586* fetus tissue shows grossly normal neuromuscular pattern in **(D)** "segment 1," with well-defined ENS plexuses, normal muscle (∼20 mm) and mucosa (∼6 mm) thickness. **(E)** "segment 2" has scattered ENS with smooth muscle (∼140 mm) and mucosa (∼25 mm) overgrowth. **(F–H)** Immunofluorescence staining for DAPI (nucleus) and CS56 (chondroitin sulfate proteoglycans) on intestine sections. **(F,G)** 26 weeks control intestine and Segment 1" with CS56 expression in the serosa, submucosa and mucosa. **(H)** "Segment 2" shows absence of CS56 staining. **(I)** Human/chicken cross-species analysis of intestinal tissues in *talpid*^{3} and KIAA0586 mutants has statistically significant increase in (i) ENS cells numbers (40.8%,$^{**}p = 0.004$) and (ii) epithelium and smooth muscle tissue thickness (77%,$^{***}p = 0.00006$ and 413%, $^{****}p < 0.0001$, respectively). **(J,K)** Immunofluorescence staining for DAPI (nucleus) and Cytokeratin on mucosal sections. **(J)** 26 weeks control intestine has uniform Cytokeratin staining in the mucosa. **(K,L)** "Segment 1 and 2" show uneven Cytokeratin expression. **(M–O)** Immunofluorescence staining for DAPI (nucleus) and Patched. **(M)** "Segment 1" has reduced submucosal staining and normal mucosal staining compared to 26 weeks control. **(O)** "Segment 2" shows no Patched staining. ctrl, control; muc, mucosa; sub muc, submucosa; cm, circular muscle; lm, longitudinal muscle; MYP, myenteric plexus; SMP, submucosal plexus. Same scale bar in **(J–O)**.

note, and again in accordance with the defects observed in the chicken model, the number of cells in both the epithelium and muscle layers was affected, in a non-cell autonomous manner, by the lack of TALPID3 in the ENCC. Indeed, quantitative analysis of cell numbers in both tissues showed statistically significant 39% increase in the epithelium ($p = 0.009$; $n = 7$ sections) and 67% increase in the muscle layers ($p = 0.002$; $n = 7$ sections), with an 80% increase in the longitudinal muscle ($p = 0.002$) and 55% increase in the circular muscle ($p = 0.018$). Interestingly, the smooth muscle myoblasts appeared misshaped in the conditional *Talpid3* mutant (**Figures 6A′–F′′,A′′–F′′** and **Supplementary Videos 1, 2**). The transgenic mouse measurements were combined with equivalent chicken data from the *talpid*^{3} > GFP transplant for mouse/chicken cross-species analysis. Cell counts for epithelium showed a statistically significant ($^{**}p = 0.009$) increase of 39% in the chimeric animals compared to controls. Smooth muscle cell count showed a highly statistically significant ($^{**}p = 0.002$) increase of 67% in chimeric animals compared to control. The relative increase observed in ENS cell numbers was not statistically significant in this cross-species analysis (**Figure 6H**). Overall, apart

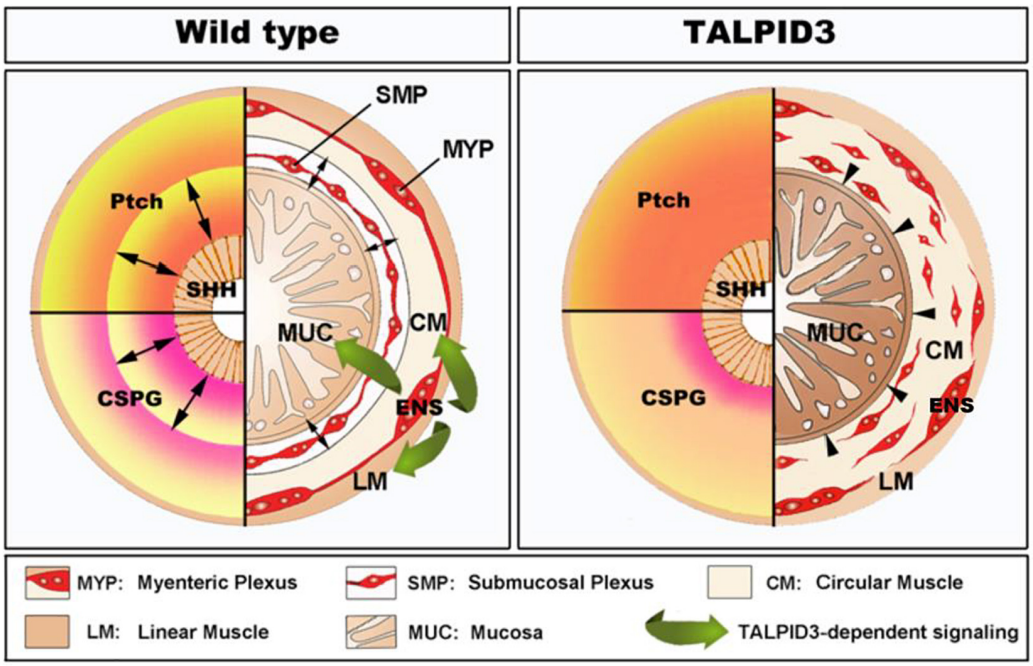

FIGURE 8 | Model of TALPID3-dependent gastrointestinal neuromuscular patterning. During normal gut development **(Left)**, the Sonic Hedgehog (SHH) gradient defines the concentric architecture of the intestine as seen by the discrete PATCHED (Ptch) pattern of expression. SHH readout in the mesenchyme immediately adjacent to the epithelium restricts smooth muscle differentiation to allow the connective tissue of the submucosa to develop. In the absence of a functional TALPID3 protein **(Right)**, the SHH readout is lost, as shown by the diffused *Ptch* expression. Loss of the SHH readout leads to ectopic spread of the smooth muscle differentiation domain adjacent to the epithelium. **(Left – bottom)** During normal gut development, the precise readout of the SHH gradient directs the pattern of CSPG expression, restricting ENCC to the locations where the enteric nervous system (ENS) will form. The ENS regulates smooth muscle and mucosa growth and differentiation *via* a TALPID3-dependent signaling (green arrows). **(Right – bottom)** In the absence of a functional TALPID3 protein, SHH readout is lost, which coincides with a loss of CSPG expression. This loss of expression permits ectopic ENCC migration resulting in scattered ENCC throughout the gut mesenchyme. Loss of TALPID3 also leads to altered growth and differentiation of smooth muscle and mucosal epithelium.

from altered cell numbers, knocking out *talpid*^{3} in ENCC had little effect on early ENS development and patterning in both chicken and mouse models, but it altered growth and differentiation of smooth muscle and mucosa in a non-cell-autonomous manner.

Human Embryonic Tissues Bearing a *KIAA0586* Mutation Recapitulate the Gastrointestinal Defects Observed in TALPID3 Animal Models

To assess whether the role of TALPID3 is conserved throughout evolution and is relevant to human GI tract development and patterning, we examined human fetal GI tissues obtained from a 26 weeks human fetus with a homozygous for a 1815G > A mutation in *KIAA0586*, the human ortholog of *talpid*^{3} *(chicken) and Talpid3 (mouse)*, as previously described (Alby et al., 2015). Previous anatomical description of the fetus listed shortened ribs, micromelia, lingual hamartomas, postaxial and preaxial polydactyly, temporal polymicrogyria and an occipital keyhole defect (Alby et al., 2015; Cocciadiferro et al., 2020). Gross examination of the GI tract revealed an elongated and tubular stomach, but otherwise apparently normal GI tract. Histological analysis showed a portion of the intestine ("segment 1") with grossly normal neuromuscular pattern (**Figures 7A,D,G**) consistent with that observed in a 26 weeks control fetus (**Figure 7C**). However, another portion (designated as "segment 2") showed massive overgrowth of the smooth muscle layers (∼140 mm in the mispatterned "segment 2," compared to ∼20 mm in "segment 1," and 26 weeks control) and the mucosa (∼25 mm in the mispatterned "segment 2," compared to ∼6 mm in "segment 1," and 26 weeks control). The smooth muscle overgrowth in "segment 2" corresponded to an increase in thickness of 6.5 times (**Figures 7B,E,H**). Additionally, immunostaining for TuJ1 showed enteric neurons scattered throughout the gut wall (**Figure 7E**), in a pattern similar to that observed in the *talpid*^{3} chicken model (**Figures 1O–R**). The striking similarities found in histological observations were confirmed by combining equivalent measurements from human and chicken intestinal tissues for human/chicken cross-species analysis. This analysis showed a statistically significant increase in (i) ENS cell numbers (40.8%,$^{**}p = 0.004$) and (ii) epithelium and smooth muscle tissue thickness (77%,$^{***}p = 0.00006$ and 413%, $^{****}p < 0.0001$, respectively) in mutant tissues compared to stage matched controls (**Figure 7I**). We also investigated expression of human chondroitin sulfate proteoglycans using CS56 (**Figures 7F–H**). 19 and 26 weeks controls showed expression of CS56 in

the serosa the submucosa and the mucosa (**Figure 7F** and **Supplementary Figure 5B**). In "segment 1," CS56 expression was also observed in the serosa and the mucosa whereas, strikingly, in "segment 2" no CS56 expression was detected (**Figures 7G,H**). To investigate further the intestinal phenotype of this fetus, we examined the expression of both Patched and Cytokeratin (**Figures 7J–O**). Even though cytokeratin was expressed in the fetus bearing the *KIAA0586* mutation, the staining was not as strong and uniform as in the control. Likewise, Patched staining was reduced in "segment 1" of the fetus bearing the *KIAA0586* mutation compared to the control, whereas "segment 2" showed no staining. The altered *patched* expression was confirmed by *in situ* hybridization (**Supplementary Figures 4C–E**). Both epithelial stainings pointed to delayed/altered gut epithelial differentiation. Overall, the phenotype observed in "segment 2" of the fetus was strikingly similar to that of the *talpid*^{3} chicken model with scattered enteric neurons, smooth muscle and mucosa overgrowth as well as impaired differentiation. Other defects observed in both human and the chicken model included: (i) altered Hh pathway (as shown by a lack of Patched expression and loss of mRNA expression pattern) (ii) impaired epithelium differentiation (as shown by Cytokeratin) and (iii) lack of CSPG components of the ECM.

DISCUSSION

Although TALPID3 has been recognized to have essential functions during embryonic development, its role during GI and ENS development has not, as yet, been studied. Previous investigations have shown that TALPID3 animals are useful to model human birth defects such as short ribs, polydactyly, or craniofacial abnormalities that are attributed to abnormal hedgehog signaling (Davey et al., 2007; Bangs et al., 2011; Ben et al., 2011; Alby et al., 2015). Our findings establish that TALPID3 animal models can also offer insights for congenital human GI defects, such as short gut, tracheoesophageal atresia/fistula, and anorectal abnormalities, i.e., a variety of defects commonly seen in pediatric gastroenterology clinics. Moreover, the striking similarities between the neuromuscular abnormalities described here, in chicken, mouse and human, demonstrate that the function of TALPID3 is well conserved across species and is of importance for normal human gut development.

TALPID3 Is a Regulator of Gastrointestinal Neuromuscular Patterning

We specifically examined the role of TALPID3 in neuromuscular patterning of the developing GI tract, as it was clear from the histological defects in both chicken and human GI tissues that lack of TALPID3 led to severe disruption of this developmental process. Our analysis showed that the lack of TALPID3 consistently affected the neuromuscular patterning of the gut. Interestingly though, the resulting phenotypes varied, depending on the location along the A–P axis of the gut. In the chicken model, lack of TALPID3 in the esophagus led to complete absence of smooth muscle and ENS, whereas in the stomach and the intestine lack of TALPID3 led to ectopic smooth muscle differentiation and misplaced enteric neurons. Likewise, one portion of the human intestine from a fetus bearing a *KIAA0586* mutation showed grossly normal neuromuscular patterning, whereas another had dramatic muscle overgrowth and scattered enteric neurons. These observation, when combined with quantifications of enteric neuronal, smooth muscle and epithelial cell numbers, suggest that, albeit with species differences, TALPID3 is part of a conserved mechanism controlling the appropriate spatial differentiation of smooth muscle and the correct positioning of enteric neurons. Moreover, TALPID3 functions as part of regional-specific mechanisms regulating the correct neuromuscular patterning at different levels of the GI tract. Perhaps this is not surprising since the spatiotemporal development of GI smooth muscle has been shown to have regional-specific differences (Bourret et al., 2017; Graham et al., 2017). Our results are in accordance with recent findings in the related chicken mutant *talpid2* (Brooks et al., 2021).

Disruption of Gastrointestinal Patterning in *talpid*^{3} Mutant Is Linked to Impairment of the Hh Pathway

Our findings add to the body of evidence linking TALPID3 to the Hh signaling pathway (Davey et al., 2007; Bangs et al., 2011; Ben et al., 2011; Alby et al., 2015; Li et al., 2017). The link between TALPID3 and Hh signaling in the gut can be observed in (i) the gross anatomy of the GI tract (ii) the smooth muscle and (iii) ENS defects of the mutants. (i) First, the gross anatomical abnormalities in the TALPID3 chicken GI tract are consistent with a loss of Hh signaling. Severe reduction in GI tract size with normal gross anatomy has been reported using a conditional approach to remove both *Shh* and *Ihh* functions from early mouse gut endoderm (Mao et al., 2010). Likewise, mouse knockouts of *Shh*, *Gli2* and *Gli3* all display tracheo-esophageal atresia/fistula, a phenotype also described here in the TALPID3 chicken mutant (Motoyama et al., 1998; Ramalho-Santos et al., 2000). Additionally, regulation of gut epithelium homeostasis has been linked to the Shh signaling pathway and both *talpid*^{3} chicken and *KIAA0585* human gut tissue showed altered epithelium growth/differentiation (Mao et al., 2010; Ben-Shahar et al., 2019). Lastly, Hedgehog signaling is critical for normal anorectal development and anorectal malformations have been reported in *shh* knockout mice and in humans with polymorphisms in Hedgehog genes (Ramalho-Santos et al., 2000; Gao et al., 2016). The open hindgut phenotype of the *talpid*^{3} chicken model offers an additional model for researching such malformations. (ii) It has been shown that Shh signaling regulates the concentric architecture of the intestine. In particular, SHH affects the mesenchyme immediately adjacent to the epithelium, where it restricts smooth muscle differentiation to allow the connective tissue of the submucosa to develop (van den Brink, 2007; Huycke et al., 2019). The increased domain of smooth muscle differentiation in the stomach and intestine of the *talpid*^{3} chicken suggests that this Hh-dependant

regulation is lost. Moreover, the results from *ptch in situ* hybridization in *talpid*^{3} mutants directly demonstrate that SHH expressed by the endoderm is not correctly integrated throughout the radially surrounding mesenchyme. The lack of PATCHED protein immunostaining in "segment 2" suggests that this part of the gut is unable to respond to SHH signaling. The loss of the proximal SHH readout in the *talpid*^{3} mutants can be directly correlated with the subsequent differentiation of smooth muscle adjacent to the epithelium in the stomach and intestine. This result demonstrates that mesenchymal cells surrounding the epithelium are competent for induction into smooth muscle, but are normally prevented from doing so by the proximal SHH gradient *via* a TALPID3-dependent mechanism. In the esophagus, the lack of TALPID3 does not lead to an extension of the smooth muscle differentiation domain, but rather to a lack of smooth muscle differentiation altogether, pointing to a different region-specific readout of the Hh signal. This failure of smooth muscle differentiation in the esophagus may explain why migrating ENCC do not halt their migration and differentiate into enteric neurons, as they lack target tissue to innervate. Indeed, ENCC were observed at the level of the esophagus at stage E6.5 in the *talpid*^{3} chicken mutant, but no cells were present in this region at E8.5. TALPID3 is therefore necessary for the correct integration of SHH throughout the gut mesenchyme and to define the concentric architecture of the smooth muscle differentiation domain. Our results fit in with a recent study showing that Hedgehog acts through Bmp signaling to inhibit subepithelial smooth muscle and that levels of Hedgehog signaling regulate differentiation of the inner smooth muscle layer (Huycke et al., 2019). This suggests that TALPID3 is part of this regulatory mechanism. (iii) The influence of SHH on NCC migration and proliferation is well established, but many paradoxical results point to a complex role for Hh during ENS development with species and developmental differences, as well as direct and indirect regulatory mechanisms (Ramalho-Santos et al., 2000; Fu et al., 2004; Reichenbach et al., 2008; Biau et al., 2013; Jin et al., 2015). Recent results clearly show, both in chicken and mouse, that the SHH receptor Patched is not expressed by ENCC and point to indirect regulatory mechanisms (Nagy et al., 2016). Our findings are in agreement with an indirect regulation of ENCC by SHH through its role in modifying the gut ECM and thereby the environment through which ENCC migrate, as we discuss below.

Loss of TALPID3 and Hh Signaling Is Associated With ECM Defects and Absence of Environmental Neural Crest Cells Repellent Cues

In search of a mechanistic explanation for the lack of ENS plexus formation in *talpid*^{3} mutants, we analyzed expression of CGPG molecules, which are components of the gut ECM. Expression of ECM components is known to be regulated by both primary cilia and Hh signaling (Seeger-Nukpezah and Golemis, 2012; Nagy et al., 2016), making them good candidates for further investigation. Alterations in ECM expression have also been described in human ciliopathies (Ramalho-Santos et al., 2000; Seeger-Nukpezah and Golemis, 2012). Importantly, CSPG molecules provide guidance cues for neuronal behaviors such as migration, axon outgrowth and axon termination (Ring et al., 1996; Carulli et al., 2005; Siebert et al., 2014). We specifically investigated Coll9, a CSPG expressed in the developing gut, which has been shown to elicit avoidance behavior by NCC *in vitro* (Ring et al., 1996; Nagy et al., 2016). In correlation with the loss of Hh signaling in the GI tract of both the *talpid*^{3} chicken and the fetus bearing a *KIAA0586* mutation, expression of CSPG molecules was lost. Importantly, double staining of CSPG and NCC showed that the disappearance of the CSPG expression correlated tightly with ectopic localization of ENCC, suggesting that the lack of repellent molecules such as Coll9 is a direct mechanism underlying the lack of ENS plexus formation in *talpid*^{3} GI tract. This finding is in agreement with previous studies showing that the regulation of CSPG by SHH in both chicken and mouse models can modify the behavior of ENCC and subsequently ENS patterning (Nagy et al., 2016). To investigate a possible connection between smooth muscle differentiation and the expression of CSPG, we performed double immunofluorescence with SMA and coll9 antibodies. We found that SMA and Coll9 have distinct, yet partially overlapping, patterns of expression. This demonstrates that some myoblasts express Coll9. However, Coll9 is mainly expressed in mesenchymal cells and it is this wider CSPG expression domain, and not the SMA domain, that correlates best with the regional localization of ENCC. Additionally, our chicken transplantation experiments demonstrated the inability of wild type ENCC to rescue ENS formation in a TALPID3-null gut environment. This finding highlights the role of environmental cues in directing ENS formation and shows that ENS plexus development does not rely on self-organizing properties of ENCC. This is in agreement with recent work showing that disruption of the ENCC environment can disrupt ENS patterning (Graham et al., 2017). Our study also demonstrates that TALPID3 expression in the gut is essential for proper expression of guidance cues that direct ENS plexus patterning. Importantly, we also show that this role is conserved during human fetal gut development.

TALPID3 Is Not Required Cell Autonomously for Enteric Nervous System Plexus Formation but Is a Regulator of Neuronal-Mesenchymal-Epithelial Interactions Directing Correct Tissue Growth and Differentiation

We investigated the cell autonomous requirement for TALPID3 during ENCC migration and gut patterning by knocking out *Talpid*^{3} specifically in ENCC, either by neural tube transplantation in chicken or using a *Wnt1-Cre* driven *Talpid*^{3} conditional knockout in mouse. In both models, TALPID3 was found not to be required for ENCC migration or normal ENS plexus formation as the gross morphology of the ENS was unaffected. The only alteration to the ENS in

these conditions was the increase in cell number observed in the chicken model and in the mouse model, which we quantified in stomach sections. Alteration of NCC numbers could be the result of subtle migration or differentiation defects changing the relative number of ENCC in specific locations. Alternatively, it could be linked to a TALPID3-dependent alteration of the SHH pathway and, specifically, the influence of SHH on NCC as a mitogen (Fu et al., 2004; Reichenbach et al., 2008; Roper et al., 2009; Nagy et al., 2016). Remarkably, knocking out *Talpid*^{3} in ENCC led to wider non-cell autonomous defects in other tissues such as smooth muscle and epithelium. Both the mouse and chicken phenotypes revealed a neural crest TALPID3-dependent mechanism controlling growth and differentiation of mesenchyme and epithelium. The most striking effect was alteration of smooth muscle differentiation and increased numbers of myoblasts which we quantified in stomach sections in chicken and mouse. The alteration of smooth muscle differentiation was particularly evident in the stomach region of mice. Variations in epithelium shape and cell numbers were also evident both in mouse, chicken. Mouse/chicken cross-species analysis confirmed that these differences in smooth muscle and epithelial cell numbers were statistically significant when comparing chimeric animals to controls. Interestingly, in addition to its role in smooth muscle development, the Hh pathway also plays an important role in mucosal growth (Mao et al., 2010; Ben-Shahar et al., 2019). Indeed *shh* and *gli3* mutant mice have mucosal hyperplasia in the stomach (Ramalho-Santos et al., 2000; Kim et al., 2005). It has been previously postulated that vagal ENCC could act as a mediator in the mesenchymal-epithelial interactions that control stomach development (Faure et al., 2015). Additionally it has been shown that ENS influences the differentiation and growth of other cell types within the gut, as demonstrated by smooth muscle overgrowth in the aganglionic portion of EdnrB mice, as well as alteration of goblet cell differentiation (Spencer et al., 2007; Thiagarajah et al., 2014). Recent work has also shown that implantation of neural crest cells within tissue-engineered small intestine altered the transcriptome of a wide variety of gastrointestinal cell types, demonstrating the necessity of the neuronal lineage to be able to recapitulate gut organogenesis *in vitro* (Schlieve et al., 2017). Our findings emphasize the importance of the neural component for correct smooth muscle and mucosa development both during embryonic gut development and for regenerative medicine research. Moreover our study shows the central role played by TALPID3 in neuronal-mesenchymal-epithelial interactions necessary for normal GI tract development.

The neural crest specific *talpid*^{3} knockout results described here are in agreement with non-cell autonomous effects seen in other tissues after NCC-specific gene knockout. For example, knocking out the intraflagellar protein Kif3a in NCC led to non-cell autonomous striated muscle defects during tongue development (Millington et al., 2017). Additionally, loss of NCC disrupts the distribution of second heart field cells in the pharyngeal and outflow regions (Bradshaw et al., 2009). Likewise, conditional neural crest Rac1 knockout, using a *Rac1/Wnt1-Cre* line, shows excessive proliferation of SMA+ cell wall around the aortic sac and ventral aorta (Waldo et al., 2005; Thomas et al., 2010). Investigating the gut phenotype of *Rac1/Wnt1-Cre* mutants for smooth muscle defects would be informative. Interestingly, Rac1 is downstream of the non-canonical SHH pathway (Mulligan, 2014). TALPID3 and Rac1 have a comparable function in vesicular trafficking (Stenmark, 2009), centrosome regulation (May et al., 2014) and in cell-matrix interactions (Thomas et al., 2010). Rac1 is also downstream of RET, a tyrosine kinase receptor essential for ENS development (Natarajan et al., 2002; Fu et al., 2010; Mulligan, 2014).

Migrating Enteric Neural Crest Cells Do Not Extend a Prominent Primary Cilia

Having established that TALPID3 was not required cell autonomously for ENCC migration and gross ENS patterning, and considering the role of TALPID3 in ciliogenesis, it follows that primary cilia might not be required for ENCC migration. ENCC are a highly proliferative cell population and it is their mitogenic activity, which is driving their migration and invasiveness (Simpson et al., 2007). It is known that there is a reciprocal regulation of cilia and the cell cycle, so that the primary cilium is dismantled in replicating cells, which makes it unlikely for highly proliferative cells to extend a primary cilium (Ishikawa and Marshall, 2011; Ford et al., 2018). Interestingly, migrating interneurons within the developing murine brain do not show an extended primary cilium (Higginbotham et al., 2012). In our study, we failed to observe primary cilia in migrating chicken vagal ENCC using *in vitro* neural tube culture. Performing Immunohistochemistry on tissue sections at E6.5, migrating ENCC bearing a primary cilium were seldom observed (11% of HuC$^+$ ENCC). It has been shown that differentiated ENS neurons bear a primary cilium (Junquera Escribano et al., 2011; Luesma et al., 2013). Other studies describe primary cilia on YFP+ cranial NCC using the *Wnt1:Cre; Rosa:YFP* transgenic line (Brugmann et al., 2010; Millington et al., 2017). In this transgenic line, YFP is expressed in both the neural tube (which is ciliated) and the neural crest derivatives. This lack of discrimination is problematic to decipher this issue (Cassiman et al., 2006; Murdoch and Copp, 2010). Our study suggests that extending primary cilia mainly happens as ENCC start to differentiate into enteric neurons and might not be required for migration *per se*.

Role of the Human TALPID3 Ortholog *KIAA0586* in Human Gastrointestinal Tract Development

KIAA0586 is the human ortholog of *talpid*^{3}. Some homozygous mutations of *KIAA0586* have been shown to be embryonic lethal and to lead to severe developmental abnormalities such as Hydrolethalus syndrome and short-rib polydactyly (Alby et al., 2015). Here we show that the phenotypic spectrum of *KIAA0586* mutations extends to defects in the GI tract. Apart from a tubular stomach the gross anatomy of the GI tract of the fetus was normal. However, our histological analysis showed severe alteration of the gut patterning with smooth

muscle and mucosa hyperplasia, as well as scattered enteric neurons in a sub-section of the intestine we designated "segment 2." In accordance with the animal models, we show that this phenotype is the consequence of disruption of the Hh pathway and loss of normal ECM expression. Our findings shed light on the central role of KIAA0586 in patterning of the gut during human fetal development. Recently *KIAA0586* mutations have also been identified in Joubert syndrome patients. JBTS is defined by three primary findings: (i) underdevelopment of the brain cerebellar vermis, (ii) brain stem defects giving the appearance of the molar tooth sign (MTS) and (iii) Hypotonia (Abdelhamed et al., 2013; Sanders et al., 2015; Stephen et al., 2015). Importantly also, patients typically have a perturbed respiratory pattern in the neonatal period and severe psychomotor delay. Although very rare, association with Hirschsprung disease and problems with bladder and bowel control (incontinence) have been reported in Joubert patients with milder forms of the disease (Shian et al., 1993; Ozyurek et al., 2008; Akhondian et al., 2013; Purkait et al., 2015). Considering the role of KIAA0586 in tissue patterning our study unfolds, it is also tempting to speculate that other symptoms of JBTS (like psychomotor delay, hypotonia and respiratory difficulties), could be linked to neuronal-mesenchymal-epithelial patterning defects in other parts of the body. Interestingly, in this study, *Wnt1:Cre; Talpid3* $^{fl/fl}$ P0 mutants died at birth from presumed respiratory failure, as their lungs did not appear to inflate. This points to a possible failure in the developmental interactions of neural crest, smooth muscle and epithelium, as lung neural crest cells share developmental origins with ENCC (Burns and Delalande, 2005; Freem et al., 2012). Finally, the ENS is often referred to as the "second brain" and it is possible that brain ECM defects, similar to the ones we describe in this study, could underlie abnormal brain patterning defects, such as cortical heterotopias, commonly seen in Joubert syndrome, but also in Bardet–Biedl syndrome or Meckel–Gruber syndrome (Willaredt et al., 2008; Abdelhamed et al., 2013; Higginbotham et al., 2013). In mice, a large variety of CSPGs represent major components of the ECM in the brain (Horii-Hayashi et al., 2015). In human, defects in ECM, leading to impaired neuronal guidance, could underlie other types of brain function abnormalities. A recent CNS conditional *Talpid*^{3} knockout mouse model for JBTS showed cerebellar defects due to granule cell proliferation, migration and differentiation, three aspects of cellular behavior also affected in our models (Bashford and Subramanian, 2019). This study, however, did not investigate ECM components.

CONCLUSION

Our findings demonstrate a central role for the centrosomal protein TALPID3 in neuromuscular patterning of the developing gastrointestinal tract (summarized in **Figure 8**). We show that the function of TALPID3 during GI neuromuscular patterning is conserved in vertebrates including during human fetal development. Our findings also reveal a new role for the ENS in regulating neuronal-mesenchymal-epithelial interactions necessary for normal GI tract development, and that this regulatory mechanism is TALPID3-dependent. These findings add new understandings to human GI tract developmental mechanisms and have direct implications for regenerative medicine, as they emphasize the importance of the neural component for *in vitro* gut organogenesis.

MATERIALS AND METHODS

Taplid^3 Chicken

Fertile chicken eggs were obtained from commercial sources within the UK. *talpid*^{3} and transgenic (http://topics.sciencedirect.com/topics/page/Green_fluorescent_protein) GFP chicken eggs were obtained from The Roslin Institute, The University of Edinburgh (McGrew et al., 2004; Davey et al., 2006). Eggs were incubated at 37°C and staged according to the embryonic day of development (E), and by using the developmental tables of Hamburger and Hamilton (Hamburger and Hamilton, 1951). The *talpid*^{3} mutation leads to leaky blood vessels causing very high mortality (Davey et al., 2006). This high mortality meant that specimens were collected over more than 10 years. Our study presents oldest time point at which we could reliably analyse gut tissues (E6.5 for most of the study). Beneficial outcrossing of the Talpid flock improved survival over time. It became possible to analyse later time points, when the gut is more developed, as shown in Figure 1 with E8.5 and E10.5 specimens.

Chicken Intraspecies Neural Tube Grafting

For each combination of grafting experiment (chick^{GFP}-*talpid*^{3}; *talpid*^{3}-chick^{GFP}; chick^{GFP}- wild type), the neural tube adjacent to somites 2–6 inclusive (and its associated neural crest) was microsurgically removed from the host embryos at embryonic day E1.5 and replaced with equivalent stage-matched tissue, as previously described (Burns and Le Douarin, 2001; Delalande et al., 2015). Following grafting, eggs were returned to the incubator, and embryos allowed to develop to the appropriate stage. To ascertain the genotype of the Talpid^3 neural tube transplant onto a GFP host embryo, the remaining tissues of the donor were used for DNA extraction, PCR amplification and sequencing of the region flanking the a366 mutation on exon7 using the following primers: Forward: CATTAGCTCTGCCGTCAACA Reverse: GGTAGGCAGACCACTGGAAG (**Figure 2**) (Davey et al., 2006). A total of 30 GFP neural tube grafts into TALPID3 hosts were made, of which 2 homozygote *talpid*^{3} mutant hosts were fixed for analysis at E6.5. After series of "blind" grafting experiments, a total of 5 *talpid*^{3} neural tube grafts onto GFP hosts were identified after genotyping, of which only 1 chimera survived and was fixed for analysis at E7.5.

Mouse Conditional Knockout

Animals used for this study were maintained and the experiments were performed in accordance with local approvals and the United Kingdom Animals (Scientific Procedures) Act, 1986

under license from the Home Office (PPL70/7500). *Talpid3*$^{f/f}$ mice were acquired from Prof. Malcolm Logan (King's College London). *Wnt1-cre;R26R-YFP/YFP* mice (Srinivas et al., 2001; Druckenbrod and Epstein, 2005), in which NCC express yellow fluorescent protein (YFP), were crossed to *Talpid3*$^{f/f}$ to generate a neural crest conditional knockout of *Talpid*^{3}. Subsequent *Wnt1:Cre; Talpid3*$^{flox/flox}$ mouse tissues were examined at postnatal day 0 (P0).

Human Embryonic and Fetal Material

Human material was sourced *via* the Joint MRC/Wellcome Trust Human Developmental Biology Resource (HDBR) under informed ethical consent with Research Tissue Bank ethical approval (08/H0712/34 + 5 and 08/H0906/21 + 5) (Gerrelli et al., 2015). Staging of embryos was carried out according to the Carnegie system. GI tissues from a fetus with Short-rib polydactyly and bearing a homozygous null mutation in *KIAA0586* were obtained from case II:5 family 4, as previously described in Alby et al. (2015). Informed consent was obtained for all participating families, and the study was approved by the ethical committee of Paris Ile de France II.

Tissue Sectioning

Transverse sections were cut from whole embryos and dissected gut segments. Sections were obtained at a thickness of 6 μm from wax blocks and 10–15 μm from frozen blocks. All sections were placed on Superfrost Plus microscope slides (BDH Laboratories).

Immunofluorescence and *in situ* Hybridization

For labeling of chicken and human dissected GI samples, the tissues were cryoprotected in 15% sucrose in PBS and frozen in liquid Nitrogen. Frozen sections were cut at 12 μm using a Leica CM1900 cryostat at −22°C. Briefly, for immunofluorescence, antibody blocking solution (10% sheep serum, 1% Triton-X-100 in PBS) was applied for 1 h at room temperature then samples were rinsed extensively in PBS and incubated primary antibodies (listed in **Table 1**) diluted in antibody blocking solution overnight at 4°C. Samples were then washed three times in PBS for 20 min and incubated with fluorescently tagged secondary antibodies (listed in **Table 2**) for 4 h at room temperature. Samples were washed for 1 h, and stained for 10 min with DAPI, before being mounted under a coverslip using Vectashield mounting medium (Vector Laboratories) as previously described (Wallace and Burns, 2005; Delalande et al., 2014) *in situ* hybridization was performed as previously described (Burns and Delalande, 2005).

Confocal Microscopy, Cell Counting and Statistical Analysis

Tissues were imaged using confocal microscopy (Zeiss LSM 710 confocal microscope). Images of gut sections double immunostained with relevant tissue antibodies and DAPI. Equivalent fields of relevant sections were examined in controls, mutants and/or chimeras (minimum $n = 3$). Cells were counted and tissue thickness measured using the Image-J Fiji cell counter plugin and measuring tool, respectively. Data was plotted to a histogram or interval plot. The results for all samples were normalized to baseline. The outcome was set as the percentage of the difference between the baseline and the experimental conditions. Multiple linear regression was used to study the effects of tissue, species and gene mutation simultaneously (Schneider et al., 2010; Lunt, 2013). This allowed us to assess the relative contribution of each predictor to the total variance that our model explained. Interaction terms were also considered with stricter p-value cut offs. The models were validated using the adjusted R squared and by performing residual analysis. To assess possible tissue rescue in the GFP > *taplid*^{3} transplantation experiment, the non-parametric Spearman's Rho test was used to measure the correlation between control, chimera and mutant. All raw data and statistical analysis calculations are available here: https://datadryad.org/stash/share/xNqbJ7teCQMoatb4CDKgsdbtIPGZ5QH1eGBvz_g-fVY.

Neural Tube Culture and Scanning Electron Microscopy

Migrating vagal NCC for scanning electron microscopy imaging were obtained using *in vitro* neural tube cultures as previously described (Delalande et al., 2008). Samples were then fixed overnight in 2% glutaraldehyde, 2% paraformaldehyde in 0.1 M phosphate buffer, pH7.4, at 4°C, post-fixed in 1% OsO_4/1.5% $K_4Fe(CN)_6$ in 0.1 M phosphate buffer at 3°C for 1.5 h. After rinsing with 0.1 M phosphate buffer and distilled water, specimens were progressively dehydrated to 100% ethanol, then washed once in acetone. The samples were then critical point dried using CO_2 and mounted on aluminum stubs using sticky

TABLE 1 | Primary antibodies for immunohistochemistry studies.

Primary antibody	Concentration	Company
Mouse anti-TuJ1	1:500	Covance (MMS-435P)
Mouse anti-CS56	1:2000	SIGMA (C8350)
Mouse anti-collagen IX	1:2	DSHB (2B9)
Mouse anti-SMA	1:400	Dako (M0851)
Chicken anti-GFP	1:500	Abcam (ab13970)
Chicken anti-Ncad	1:5	DSHB (6B3)
Rabbit anti-SHH	1:400	Santa Cruz (sc-6149)
Rabbit anti-PTCH	1:100	EMD Millipore (06-1102)
Rabbit anti-IFT88	1:400	Thermo Fisher (PA56997)
Pan cytokeratin-488	1:20	eBioscience (53-9003-82)
Rabbit anti-Arl13b	1:50	ProteinTech (17711-1-AP)

TABLE 2 | Secondary antibodies for immunohistochemistry studies.

Secondary antibody	Alexa fluor	Concentration	Company
Goat anti-rabbit	488	1:500	Invitrogen
Goat anti-mouse	488	1:500	Invitrogen
Anti-chicken	488	1:500	Abcam
Anti-mouse	568	1:500	Invitrogen
Anti-rabbit	568	1:500	Invitrogen
Anti-mouse	647	1:500	Invitrogen
Anti-rabbit	647	1:500	Invitrogen

carbon taps. Samples were then coated with a thin layer of Au/Pd (2 nm thick) using a Gatan ion beam coater and imaged with a Jeol JSM-6480LV high-performance, Variable Pressure Analytical Scanning Electron Microscope.

Mouse Skeletal Staining

Wnt1:Cre; Talpid3$^{fl/fl}$ P0 mice and control littermates were fixed in 90% ethanol, then skinned and eviscerated. Staining with Alcian Blue (0.05%) was performed in 70% ethanol with 20% acetic acid, followed by staining with Alizarin Red (0.15%) in 1% KOH. Soft tissue was cleared with 1% KOH with 20% glycerol and skeletons were stored in 80% glycerol.

DATA AVAILABILITY STATEMENT

The datasets presented in this study can be found in online repositories. The names of the repository/repositories and accession number(s) can be found in the article/**Supplementary Material**.

ETHICS STATEMENT

The studies involving human participants were reviewed and approved by MRC/Wellcome Trust Human Developmental Biology Resource (HDBR) under informed ethical consent with Research Tissue Bank ethical approval (08/H0712/34 + 5 and 08/H0906/21 + 5) Ethical Committee of Paris Ile de France II. The patients/participants provided their written informed consent to participate in this study. The animal study was reviewed and approved by local approvals and the United Kingdom Animals (Scientific Procedures) Act 1986 under license from the Home Office (PPL70/7500).

AUTHOR CONTRIBUTIONS

AB, NT, and JD designed the study. AB and JD performed the chicken chimera transplantation experiments. JD, NN, DD, AG, and RH contributed and/or performed the immunohistochemistry analysis. JD, JC, AC, and GC performed *in situ* hybridization experiments. PK performed all the statistical analysis. JD, DN, and CM performed to the mouse experiments. ML provided mouse strains. NL, ST, CA, TA-B, and SL provided human samples. AB, JD, and NN analyzed the data. JD and AB wrote the manuscript with input from all authors. All authors contributed to the article and approved the submitted version.

ACKNOWLEDGMENTS

This article is dedicated to the memory of RH. We would like to thank Dagan Jenkins for the IFT88 antibody, Mark Turmaine for assistance with SEM, Kevin Lee and Erwin Pauws for assistance with cartilage and bone staining as well as help with the phenotype analysis. We also thank Jan Soetaert and Belén Martín-Martín for help with microscopy. MD and the TALPID3 flock are supported by an Institutional Strategic Grant (ISP) to The Roslin Institute from the BBSRC. NN was supported by a Bolyai Fellowship and Hungarian Science Foundation NKFI grant (124740). CM was supported by Guts UK (Derek Butler Fellowship). We are grateful to the French Society of Fetal Pathology (SoFFoet) for participating in the study. We acknowledge the NIHR Great Ormond Street Hospital Biomedical Research Centre which supports all research at Great Ormond Street Hospital NHS Foundation Trust and UCL Great Ormond Street Institute of Child Health. The views expressed are those of the authors and not necessarily those of the NHS, the NIHR or the Department of Health.

SUPPLEMENTARY MATERIAL

The Supplementary Material for this article can be found online at: https://www.frontiersin.org/articles/10.3389/fnmol.2021.757646/full#supplementary-material

Supplementary Figure 1 | Migrating ENCCs do not extend a primary cilium. **(A–C)** Scanning electron microscopy of neural tube culture and migrating vagal neural crest after 18 h culture. **(A)** Low magnification of picture shows neural tube and migrating vagal neural crest spreading out. **(B)** Close up of the neural tube shows primary cilia on cells (pseudocolored in purple, black arrows). **(C)** Close up of migrating vagal NCC shows no primary cilium. **(D)** Immunofluorescent staining for acetylated α-tubulin (green) and intraflagellar transport protein 88 (red) shows colocalization at the centrosome and no primary cilium on migrating vagal NCC (white arrow). **(E)** *In vivo* staining for the primary cilia with Arl13b on E6.5 gut sections shows signal in all mesenchymal gut cells. In migrating HuC^{+} (green) ENCCs, 11% show an extended primary cilium (inset; 10 out of 85 HuC^{+} cells counted, $n = 7$ sections). **(F)** No primary cilia staining is observed in any cell type on *talpid*^{3} E6.5 gut section.

Supplementary Figure 2 | The protein Sonic Hedgehog is expressed in both control and *talpid*^{3} intestine. **(A,B)** Immunofluorescent staining of intestine with SHH and HNK1 in **(A)** E6.5 control and **(B)** *talpid*^{3} mutant embryo. SHH (red) is expressed in the epithelium of both samples. Scattered HNK1 + ENCC (green) are observed in the intestine of *talpid*^{3} mutant embryo.

Supplementary Figure 3 | Transplantation of wild type ENCCs does not rescue the muscle phenotype in GFP > *talpid*^{3} chimeric E6.5 embryo. Measurements of epithelium (DAPI) and smooth muscle (Phalloidin) thickness in stomach and intestine sections were normalized to baseline. At E6.5 there was no statistical difference between the thickness of the epithelium of controls versus GFP > *talpid*^{3} chimera or *talpid*^{3} mutants. Thickness of the smooth muscle, as measured by phalloidin was increased 100% in the chimera and 115% in the mutant compared to GFP > wild type control transplant. Measurements of phalloidin thickness in GFP > *talpid*^{3} chimera and mutant were statistically equivalent and they were both statistically significant from the baseline control (***$p < 0.001$). ctrl, control.

Supplementary Figure 4 | Cranial and GI tract phenotypes of *Wnt1:Cre;Talpid3*$^{fl/fl}$ P0 mice and control littermate. **(A,D)** Gross phenotype of **(A)** control littermate and **(D)** *Wnt1:Cre;Talpid3*$^{fl/fl}$ P0 pups. **(B,E)** Gross morphology of the dissected gastrointestinal tract and lungs of **(B)** control littermate and **(E)** *Wnt1:Cre;Talpid3*$^{fl/fl}$ P0 pups. Mutant littermates show grossly normal GI tract, red colored uninflated lungs as well as craniofacial abnormalities such as cleft pallet, short snot and brachycephaly. **(C,F)** Skeletal staining of the skulls of **(C)** control littermate and **(F)** *Wnt1:Cre;Talpid3*$^{fl/fl}$ P0 pups. Red indicates bone and blue indicates cartilage. **(F)** *Wnt1:Cre;Talpid3*$^{fl/fl}$ skull shows frontonasal hypoplasia, hypoplastic NCC derivatives, micrognathia, facial cleft-partitioning of the nasal cartilage and underdeveloped sagittal suture.

Supplementary Figure 5 | Expression of SMA, Tuj-1, CS56 and *patched* in week 19 control human gut and *patched in situ* hybridization in 26 weeks KIAA0586 gut.

(A,B) Control intestine shows normal neuromuscular patterning and CS56 expression at week 19. **(C–E)** *In situ* hybridization against *patched* in week 19 control and *KIAA0586* mutated tissue. (C + insets) Week 19 control intestine shows strong expression of *patched* in the epithelium, in the myenteric plexus of the ENS and to a lesser extend in the smooth muscle. **(D)** "Segment 1" shows *patched* expression in the myenteric plexus (inset) and the muscle layers. **(E)** "Segment 2" shows a diffuse *patched* expression throughout the section. muc, mucosa; sub muc, submucosa; cm, circular muscle; lm, longitudinal muscle; MYP, myenteric plexus; sero, serosa.

Supplementary Video 1 | Animated confocal *Z* stack of whole mount immunofluorescent staining for SMA smooth muscle actin (red) and TuJ-1 Neuron-specific class III beta-tubulin (green) and DAPI (blue) on stomach of control P0 mice littermate **(Left)** and *Wnt1:Cre;Talpid3*$^{fl/fl}$ **(Right)**.

Supplementary Video 2 | Animated confocal *Z* stack of whole mount immunofluorescent staining for SMA smooth muscle actin (red) and TuJ-1 Neuron-specific class III beta-tubulin (green) and DAPI (blue) on intestine of control P0 mice littermate **(Left)** and *Wnt1:Cre;Talpid3* $^{fl/fl}$ **(Right)**.

REFERENCES

Abdelhamed, Z. A., Wheway, G., Szymanska, K., Natarajan, S., Toomes, C., Inglehearn, C., et al. (2013). Variable expressivity of ciliopathy neurological phenotypes that encompass Meckel-Gruber syndrome and Joubert syndrome is caused by complex de-regulated ciliogenesis, Shh and Wnt signalling defects. *Hum. Mol. Genet.* 22, 1358–1372. doi: 10.1093/hmg/dds546

Akawi, N., McRae, J., Ansari, M., Balasubramanian, M., Blyth, M., Brady, A. F., et al. (2015). Discovery of four recessive developmental disorders using probabilistic genotype and phenotype matching among 4,125 families. *Nat. Genet.* 47, 1363–1369. doi: 10.1038/ng.3410

Akhondian, J., Ashrafzadeh, F., Beiraghi Toosi, M., Moazen, N., Mohammadpoor, T., and Karami, R. (2013). Joubert Syndrome in Three Children in A Family: a Case Series. *Iran. J. Child Neurol.* 7, 39–42.

Alby, C., Malan, V., Boutaud, L., Marangoni, M. A., Bessieres, B., Bonniere, M., et al. (2016). Clinical, genetic and neuropathological findings in a series of 138 fetuses with a corpus callosum malformation. *Birth Defects Res. A Clin. Mol. Teratol.* 106, 36–46. doi: 10.1002/bdra.23472

Alby, C., Piquand, K., Huber, C., Megarbane, A., Ichkou, A., Legendre, M., et al. (2015). Mutations in KIAA0586 Cause Lethal Ciliopathies Ranging from a Hydrolethalus Phenotype to Short-Rib Polydactyly Syndrome. *Am. J. Hum. Genet.* 97, 311–318. doi: 10.1016/j.ajhg.2015.06.003

Bachmann-Gagescu, R., Phelps, I. G., Dempsey, J. C., Sharma, V. A., Ishak, G. E., Boyle, E. A., et al. (2015). KIAA0586 is Mutated in Joubert Syndrome. *Hum. Mutat.* 36, 831–835.

Bangs, F., Antonio, N., Thongnuek, P., Welten, M., Davey, M. G., Briscoe, J., et al. (2011). Generation of mice with functional inactivation of talpid3, a gene first identified in chicken. *Development* 138, 3261–3272. doi: 10.1242/dev.063602

Bashford, A. L., and Subramanian, V. (2019). Mice with a conditional deletion of Talpid3 (KIAA0586) - a model for Joubert syndrome. *J. Pathol.* 248, 396–408. doi: 10.1002/path.5271

Ben, J., Elworthy, S., Ng, A. S., van Eeden, F., and Ingham, P. W. (2011). Targeted mutation of the talpid3 gene in zebrafish reveals its conserved requirement for ciliogenesis and Hedgehog signalling across the vertebrates. *Development* 138, 4969–4978. doi: 10.1242/dev.070862

Ben-Shahar, Y., Pollak, Y., Bitterman, A., Coran, A. G., Bejar, I. N., and Sukhotnik, I. (2019). Sonic hedgehog signaling controls gut epithelium homeostasis following intestinal ischemia-reperfusion in a rat. *Pediatr. Surg. Int.* 35, 255–261. doi: 10.1007/s00383-018-4406-2

Biau, S., Jin, S., and Fan, C.-M. (2013). Gastrointestinal defects of the *Gas1* mutant involve dysregulated Hedgehog and Ret signaling. *Biol. Open* 2, 144–155.

Bourret, A., Chauvet, N., de Santa Barbara, P., and Faure, S. (2017). Colonic mesenchyme differentiates into smooth muscle before its colonization by vagal enteric neural crest-derived cells in the chick embryo. *Cell Tissue Res.* 368, 503–511. doi: 10.1007/s00441-017-2577-0

Bradshaw, L., Chaudhry, B., Hildreth, V., Webb, S., and Henderson, D. J. (2009). Dual role for neural crest cells during outflow tract septation in the neural crest-deficient mutant Splotch2H. *J. Anat.* 214, 245–257. doi: 10.1111/j.1469-7580.2008.01028.x

Briscoe, J., and Therond, P. P. (2013). The mechanisms of Hedgehog signalling and its roles in development and disease. *Nat. Rev. Mol. Cell Biol.* 14, 416–429.

Brooks, E. C., Bonatto Paese, C. L., Carroll, A. H., Struve, J. N., Nagy, N., and Brugmann, S. A. (2021). Mutation in the Ciliary Protein C2CD3 Reveals Organ-Specific Mechanisms of Hedgehog Signal Transduction in Avian Embryos. *J. Dev. Biol.* 9:12. doi: 10.3390/jdb9020012

Brugmann, S. A., Allen, N. C., James, A. W., Mekonnen, Z., Madan, E., and Helms, J. A. (2010). A primary cilia-dependent etiology for midline facial disorders. *Hum. Mol. Genet.* 19, 1577–1592. doi: 10.1093/hmg/ddq030

Burns, A. J., and Delalande, J. M. (2005). Neural crest cell origin for intrinsic ganglia of the developing chicken lung. *Dev. Biol.* 277, 63–79. doi: 10.1016/j.ydbio.2004.09.006

Burns, A. J., and Le Douarin, N. M. (2001). Enteric nervous system development: analysis of the selective developmental potentialities of vagal and sacral neural crest cells using quail-chick chimeras. *Anat. Rec.* 262, 16–28. doi: 10.1002/1097-0185(20010101)262:1<16::AID-AR1007>3.0.CO;2-O

Buxton, P., Davey, M. G., Paton, I. R., Morrice, D. R., Francis-West, P. H., Burt, D. W., et al. (2004). Craniofacial development in the talpid3 chicken mutant. *Differentiation* 72, 348–362.

Carulli, D., Laabs, T., Geller, H. M., and Fawcett, J. W. (2005). Chondroitin sulfate proteoglycans in neural development and regeneration. *Curr. Opin. Neurobiol.* 15, 116–120.

Cassiman, D., Barlow, A., Vander Borght, S., Libbrecht, L., and Pachnis, V. (2006). Hepatic stellate cells do not derive from the neural crest. *J. Hepatol.* 44, 1098–1104.

Cocciadiferro, D., Agolini, E., Digilio, M. C., Sinibaldi, L., Castori, M., Silvestri, E., et al. (2020). The splice c.1815G>A variant in KIAA0586 results in a phenotype bridging short-rib-polydactyly and oral-facial-digital syndrome: a case report and literature review. *Medicine* 99:e19169. doi: 10.1097/MD.0000000000019169

Danielian, P. S., Muccino, D., Rowitch, D. H., Michael, S. K., and McMahon, A. P. (1998). Modification of gene activity in mouse embryos in utero by a tamoxifen-inducible form of Cre recombinase. *Curr. Biol.* 8, 1323–1322.

Davey, M. G., James, J., Paton, I. R., Burt, D. W., and Tickle, C. (2007). Analysis of talpid3 and wild-type chicken embryos reveals roles for Hedgehog signalling in development of the limb bud vasculature. *Dev. Biol.* 301, 155–165. doi: 10.1016/j.ydbio.2006.08.017

Davey, M. G., McTeir, L., Barrie, A. M., Freem, L. J., and Stephen, L. A. (2014). Loss of cilia causes embryonic lung hypoplasia, liver fibrosis, and cholestasis in the talpid3 ciliopathy mutant. *Organogenesis* 10, 177–185. doi: 10.4161/org.28819

Davey, M. G., Paton, I. R., Yin, Y., Schmidt, M., Bangs, F. K., Morrice, D. R., et al. (2006). The chicken talpid3 gene encodes a novel protein essential for Hedgehog signaling. *Genes Dev.* 20, 1365–1377. doi: 10.1101/gad.369106

Delalande, J.-M., Barlow, A. J., Thomas, A. J., Wallace, A. S., Thapar, N., Erickson, C. A., et al. (2008). The receptor tyrosine kinase RET regulates hindgut colonization by sacral neural crest cells. *Dev. Biol.* 313, 279–292. doi: 10.1016/j.ydbio.2007.10.028

Delalande, J.-M., Natarajan, D., Vernay, B., Finlay, M., Ruhrberg, C., Thapar, N., et al. (2014). Vascularisation is not necessary for gut colonisation by enteric neural crest cells. *Dev. Biol.* 385, 220–229.

Delalande, J. M., Thapar, N., and Burns, A. J. (2015). Dual labeling of neural crest cells and blood vessels within chicken embryos using Chick(GFP) neural tube grafting and carbocyanine dye DiI injection. *J. Vis. Exp.* 99:e52514. doi: 10.3791/52514

Druckenbrod, N. R., and Epstein, M. L. (2005). The pattern of neural crest advance in the cecum and colon. *Dev. Biol.* 287, 125–133. doi: 10.1016/j.ydbio.2005.08.040

Faure, S., McKey, J., Sagnol, S., and de Santa Barbara, P. (2015). Enteric neural crest cells regulate vertebrate stomach patterning and differentiation. *Development* 142, 331–342.

Ford, M. J., Yeyati, P. L., Mali, G. R., Keighren, M. A., Waddell, S. H., Mjoseng, H. K., et al. (2018). A Cell/Cilia Cycle Biosensor for Single-Cell Kinetics Reveals Persistence of Cilia after G1/S Transition Is a General Property in Cells and Mice. *Dev. Cell* 47, 509–523.e5. doi: 10.1016/j.devcel.2018.10.027

Fraser, A. M., and Davey, M. G. (2019). TALPID3 in Joubert syndrome and related ciliopathy disorders. *Curr. Opin. Genet. Dev.* 56, 41–48. doi: 10.1016/j.gde.2019.06.010

Freem, L. J., Delalande, J. M., Campbell, A. M., Thapar, N., and Burns, A. J. (2012). Lack of organ specific commitment of vagal neural crest cell derivatives as shown by back-transplantation of GFP chicken tissues. *Int. J. Dev. Biol.* 56, 245–254. doi: 10.1387/ijdb.113438lf

Fu, M., Lui, V. C., Sham, M. H., Pachnis, V., and Tam, P. K. (2004). Sonic hedgehog regulates the proliferation, differentiation, and migration of enteric neural crest cells in gut. *J. Cell Biol.* 166, 673–684.

Fu, M., Sato, Y., Lyons-Warren, A., Zhang, B., Kane, M. A., Napoli, J. L., et al. (2010). Vitamin A facilitates enteric nervous system precursor migration by reducing Pten accumulation. *Development* 137, 631–640. doi: 10.1242/dev.040550

Fukuda, K., and Yasugi, S. (2002). Versatile roles for sonic hedgehog in gut development. *J. Gastroenterol.* 37, 239–246. doi: 10.1007/s005350200030

Gao, H., Wang, D., Bai, Y., Zhang, J., Wu, M., Mi, J., et al. (2016). Hedgehog gene polymorphisms are associated with the risk of Hirschsprung's disease and anorectal malformation in a Chinese population. *Mol. Med. Rep.* 13, 4759–4766. doi: 10.3892/mmr.2016.5139

Gerrelli, D., Lisgo, S., Copp, A. J., and Lindsay, S. (2015). Enabling research with human embryonic and fetal tissue resources. *Development* 142, 3073–3076. doi: 10.1242/dev.122820

Goldstein, A. M., Hofstra, R. M., and Burns, A. J. (2013). Building a brain in the gut: development of the enteric nervous system. *Clin. Genet.* 83, 307–316. doi: 10.1111/cge.12054

Graham, H. K., Maina, I., Goldstein, A. M., and Nagy, N. (2017). Intestinal smooth muscle is required for patterning the enteric nervous system. *J. Anat.* 230, 567–574. doi: 10.1111/joa.12583

Hamburger, V., and Hamilton, H. L. (1951). A series of normal stages in the development of the chick embryo. *J. Morphol.* 88, 49–92. doi: 10.1002/jmor.1050880104

Higginbotham, H., Eom, T. Y., Mariani, L. E., Bachleda, A., Hirt, J., Gukassyan, V., et al. (2012). Arl13b in primary cilia regulates the migration and placement of interneurons in the developing cerebral cortex. *Dev. Cell* 23, 925–938. doi: 10.1016/j.devcel.2012.09.019

Higginbotham, H., Guo, J., Yokota, Y., Umberger, N. L., Su, C. Y., Li, J., et al. (2013). Arl13b-regulated cilia activities are essential for polarized radial glial scaffold formation. *Nat. Neurosci.* 16, 1000–1007. doi: 10.1038/nn.3451

Horii-Hayashi, N., Sasagawa, T., Matsunaga, W., and Nishi, M. (2015). Development and Structural Variety of the Chondroitin Sulfate Proteoglycans-Contained Extracellular Matrix in the Mouse Brain. *Neural Plast.* 2015:256389. doi: 10.1155/2015/256389

Huycke, T. R., Miller, B. M., Gill, H. K., Nerurkar, N. L., Sprinzak, D., Mahadevan, L., et al. (2019). Genetic and Mechanical Regulation of Intestinal Smooth Muscle Development. *Cell* 179, 90–105.e21. doi: 10.1016/j.cell.2019.08.041

Ingham, P. W. (2016). Drosophila Segment Polarity Mutants and the Rediscovery of the Hedgehog Pathway Genes. *Curr. Top. Dev. Biol.* 116, 477–488. doi: 10.1016/bs.ctdb.2016.01.007

Ishikawa, H., and Marshall, W. F. (2011). Ciliogenesis: building the cell's antenna. *Nat. Rev. Mol. Cell Biol.* 12, 222–234. doi: 10.1038/nrm3085

Jin, S., Martinelli, D. C., Zheng, X., Tessier-Lavigne, M., and Fan, C. M. (2015). Gas1 is a receptor for sonic hedgehog to repel enteric axons. *Proc. Natl. Acad. Sci. U. S. A.* 112, E73–E80. doi: 10.1073/pnas.1418629112

Junquera Escribano, C., Cantarero Carmona, I., Luesma Bartolome, M. J., Soriano-Navarro, M., Martinez-Ciriano, C., Castiella Muruzabal, T., et al. (2011). The primary cilium: a relevant characteristic in interstitial cells of rat duodenum enteric plexus. *Histol. Histopathol.* 26, 461–470. doi: 10.14670/HH-26.461

Kang, J.-S., Zhang, W., and Krauss, R. S. (2007). Hedgehog Signaling: cooking with Gas1. *Sci. STKE* 2007:e50. doi: 10.1126/stke.4032007pe50

Kim, J., Kato, M., and Beachy, P. A. (2009). Gli2 trafficking links Hedgehog-dependent activation of Smoothened in the primary cilium to transcriptional activation in the nucleus. *Proc. Natl. Acad. Sci. U. S. A.* 106, 21666–21671. doi: 10.1073/pnas.0912180106

Kim, J. H., Huang, Z., and Mo, R. (2005). Gli3 null mice display glandular overgrowth of the developing stomach. *Dev. Dyn.* 234, 984–991. doi: 10.1002/dvdy.20542

Kobayashi, T., Kim, S., Lin, Y. C., Inoue, T., and Dynlacht, B. D. (2014). The CP110-interacting proteins Talpid3 and Cep290 play overlapping and distinct roles in cilia assembly. *J. Cell Biol.* 204, 215–229. doi: 10.1083/jcb.201304153

Li, J., Wang, C., Wu, C., Cao, T., Xu, G., Meng, Q., et al. (2017). PKA-mediated Gli2 and Gli3 phosphorylation is inhibited by Hedgehog signaling in cilia and reduced in Talpid3 mutant. *Dev. Biol.* 429, 147–157. doi: 10.1016/j.ydbio.2017.06.035

Luesma, M. J., Cantarero, I., Castiella, T., Soriano, M., Garcia-Verdugo, J. M., and Junquera, C. (2013). Enteric neurons show a primary cilium. *J. Cell. Mol. Med.* 17, 147–153. doi: 10.1111/j.1582-4934.2012.01657.x

Lunt, M. (2013). Introduction to statistical modelling 2: categorical variables and interactions in linear regression. *Rheumatology* 54, 1141–1144. doi: 10.1093/rheumatology/ket172

Mahjoub, M. R. (2013). The importance of a single primary cilium. *Organogenesis* 9, 61–69. doi: 10.4161/org.25144

Malicdan, M. C., Vilboux, T., Stephen, J., Maglic, D., Mian, L., Konzman, D., et al. (2015). Mutations in human homologue of chicken talpid3 gene (KIAA0586) cause a hybrid ciliopathy with overlapping features of Jeune and Joubert syndromes. *J. Med. Genet.* 52, 830–839. doi: 10.1136/jmedgenet-2015-103316

Mao, J., Kim, B.-M., Rajurkar, M., Shivdasani, R. A., and McMahon, A. P. (2010). Hedgehog signaling controls mesenchymal growth in the developing mammalian digestive tract. *Development* 137, 1721–1729. doi: 10.1242/dev.044586

Matsubara, Y., Nakano, M., Kawamura, K., Tsudzuki, M., Funahashi, J.-I., Agata, K., et al. (2016). Inactivation of Sonic Hedgehog Signaling and Polydactyly in Limbs of Hereditary Multiple Malformation, a Novel Type of Talpid Mutant. *Front. Cell Dev. Biol.* 4:149. doi: 10.3389/fcell.2016.00149

May, M., Schelle, I., Brakebusch, C., Rottner, K., and Genth, H. (2014). Rac1-dependent recruitment of PAK2 to G2 phase centrosomes and their roles in the regulation of mitotic entry. *Cell Cycle* 13, 2211–2221. doi: 10.4161/cc.29279

May-Simera, H. L., Gumerson, J. D., Gao, C., Campos, M., Cologna, S. M., Beyer, T., et al. (2016). Loss of MACF1 Abolishes Ciliogenesis and Disrupts Apicobasal Polarity Establishment in the Retina. *Cell Rep.* 17, 1399–1413. doi: 10.1016/j.celrep.2016.09.089

McGrew, M. J., Sherman, A., Ellard, F. M., Lillico, S. G., Gilhooley, H. J., Kingsman, A. J., et al. (2004). Efficient production of germline transgenic chickens using lentiviral vectors. *EMBO Rep.* 5, 728–733.

Merchant, J. L. (2012). Hedgehog signalling in gut development, physiology and cancer. *J. Physiol.* 590, 421–432.

Millington, G., Elliott, K. H., Chang, Y.-T., Chang, C.-F., Dlugosz, A., and Brugmann, S. A. (2017). Cilia-dependent GLI processing in neural crest cells is required for tongue development. *Dev. Biol.* 424, 124–137. doi: 10.1016/j.ydbio.2017.02.021

Motoyama, J., Liu, J., Mo, R., Ding, Q., Post, M., and Hui, C. C. (1998). Essential function of Gli2 and Gli3 in the formation of lung, trachea and oesophagus. *Nat. Genet.* 20, 54–57.

Mulligan, L. M. (2014). RET revisited: expanding the oncogenic portfolio. *Nat. Rev. Cancer* 14, 173–186. doi: 10.1038/nrc3680

Murdoch, J. N., and Copp, A. J. (2010). The relationship between Sonic hedgehog signalling, cilia and neural tube defects. *Birth Defects Res. A Clin. Mol. Teratol.* 88, 633–652.

Nagy, N., Barad, C., Graham, H. K., Hotta, R., Cheng, L. S., Fejszak, N., et al. (2016). Sonic hedgehog controls enteric nervous system development by patterning the extracellular matrix. *Development* 143, 264–275. doi: 10.1242/dev.128132

Nagy, N., and Goldstein, A. M. (2017). Enteric nervous system development: a crest cell's journey from neural tube to colon. *Semin. Cell Dev. Biol.* 66, 94–106. doi: 10.1016/j.semcdb.2017.01.006

Naharros, I. O., Cristian, F. B., Zang, J., Gesemann, M., Ingham, P. W., Neuhauss, S. C. F., et al. (2018). The ciliopathy protein TALPID3/KIAA0586 acts upstream of Rab8 activation in zebrafish photoreceptor outer segment formation and maintenance. *Sci. Rep.* 8:2211.

Natarajan, D., Marcos-Gutierrez, C., Pachnis, V., and de Graaff, E. (2002). Requirement of signalling by receptor tyrosine kinase RET for the directed migration of enteric nervous system progenitor cells during mammalian embryogenesis. *Development* 129, 5151–5160. doi: 10.1242/dev.129.22.5151

Noah, T. K., Donahue, B., and Shroyer, N. F. (2011). Intestinal development and differentiation. *Exp. Cell Res.* 317, 2702–2710.

Ozyurek, H., Kayacik, O. E., Gungor, O., and Karagoz, F. (2008). Rare association of Hirschsprung's disease and Joubert syndrome. *Eur. J. Pediatr.* 167, 475–477.

Pan, Y., Wang, C., and Wang, B. (2009). Phosphorylation of Gli2 by protein kinase A is required for Gli2 processing and degradation and the Sonic Hedgehog-regulated mouse development. *Dev. Biol.* 326, 177–189. doi: 10.1016/j.ydbio.2008.11.009

Pathi, S., Pagan-Westphal, S., Baker, D. P., Garber, E. A., Rayhorn, P., Bumcrot, D., et al. (2001). Comparative biological responses to human Sonic, Indian, and Desert hedgehog. *Mech. Dev.* 106, 107–117.

Purkait, R., Basu, R., Das, R., and Chatterjee, U. (2015). Association of Joubert syndrome and Hirschsprung disease. *Indian Pediatr.* 52, 61–62.

Ramalho-Santos, M., Melton, D. A., and McMahon, A. P. (2000). Hedgehog signals regulate multiple aspects of gastrointestinal development. *Development* 127, 2763–2772.

Ramsbottom, S. A., and Pownall, M. E. (2016). Regulation of Hedgehog Signalling Inside and Outside the Cell. *J. Dev. Biol.* 4:23.

Rao, M., and Gershon, M. D. (2016). The bowel and beyond: the enteric nervous system in neurological disorders. *Nat. Rev. Gastroenterol. Hepatol.* 13, 517–528.

Reichenbach, B., Delalande, J. M., Kolmogorova, E., Prier, A., Nguyen, T., Smith, C. M., et al. (2008). Endoderm-derived Sonic hedgehog and mesoderm Hand2 expression are required for enteric nervous system development in zebrafish. *Dev. Biol.* 318, 52–64. doi: 10.1016/j.ydbio.2008.02.061

Ring, C., Hassell, J., and Halfter, W. (1996). Expression pattern of collagen IX and potential role in the segmentation of the peripheral nervous system. *Dev. Biol.* 180, 41–53. doi: 10.1006/dbio.1996.0283

Roosing, S., Hofree, M., Kim, S., Scott, E., Copeland, B., Romani, M., et al. (2015). Functional genome-wide siRNA screen identifies KIAA0586 as mutated in Joubert syndrome. *Elife* 4:e06602. doi: 10.7554/eLife.06602

Roper, R. J., VanHorn, J. F., Cain, C. C., and Reeves, R. H. (2009). A neural crest deficit in Down syndrome mice is associated with deficient mitotic response to Sonic hedgehog. *Mech. Dev.* 126, 212–219. doi: 10.1016/j.mod.2008.11.002

Sanders, A. A., de Vrieze, E., Alazami, A. M., Alzahrani, F., Malarkey, E. B., Sorusch, N., et al. (2015). KIAA0556 is a novel ciliary basal body component mutated in Joubert syndrome. *Genome Biol.* 16:293. doi: 10.1186/s13059-015-0858-z

Sasai, N., and Briscoe, J. (2012). Primary cilia and graded Sonic Hedgehog signaling. *Wiley Interdiscip. Rev. Dev. Biol.* 1, 753–772.

Sasselli, V., Pachnis, V., and Burns, A. J. (2012). The enteric nervous system. *Dev. Biol.* 366, 64–73.

Schlieve, C. R., Fowler, K. L., Thornton, M., Huang, S., Hajjali, I., Hou, X., et al. (2017). Neural Crest Cell Implantation Restores Enteric Nervous System Function and Alters the Gastrointestinal Transcriptome in Human Tissue-Engineered Small Intestine. *Stem Cell Rep.* 9, 883–896. doi: 10.1016/j.stemcr.2017.07.017

Schneider, A., Hommel, G., and Blettner, M. (2010). Linear regression analysis: part 14 of a series on evaluation of scientific publications. *Dtsch. Arztebl. Int.* 107, 776–782. doi: 10.3238/arztebl.2010.0776

Schock, E. N., Chang, C. F., Youngworth, I. A., Davey, M. G., Delany, M. E., and Brugmann, S. A. (2016). Utilizing the chicken as an animal model for human craniofacial ciliopathies. *Dev. Biol.* 415, 326–337. doi: 10.1016/j.ydbio.2015.10.024

Seeger-Nukpezah, T., and Golemis, E. A. (2012). The extracellular matrix and ciliary signaling. *Curr. Opin. Cell Biol.* 24, 652–661.

Shian, W. J., Chi, C. S., Mak, S. C., and Chen, C. H. (1993). Joubert syndrome in Chinese infants and children: a report of four cases. *Zhonghua Yi Xue Za Zhi* 52, 342–345.

Siebert, J. R., Conta Steencken, A., and Osterhout, D. J. (2014). Chondroitin sulfate proteoglycans in the nervous system: inhibitors to repair. *Biomed Res. Int.* 2014:845323.

Simpson, M. J., Zhang, D. C., Mariani, M., Landman, K. A., and Newgreen, D. F. (2007). Cell proliferation drives neural crest cell invasion of the intestine. *Dev. Biol.* 302, 553–568. doi: 10.1016/j.ydbio.2006.10.017

Spencer, N. J., Bayguinov, P., Hennig, G. W., Park, K. J., Lee, H. T., Sanders, K. M., et al. (2007). Activation of neural circuitry and Ca2+ waves in longitudinal and circular muscle during CMMCs and the consequences of rectal aganglionosis in mice. *Am. J. Physiol. Gastrointest. Liver Physiol.* 292, G546–G555. doi: 10.1152/ajpgi.00352.2006

Srinivas, S., Watanabe, T., Lin, C. S., William, C. M., Tanabe, Y., Jessell, T. M., et al. (2001). Cre reporter strains produced by targeted insertion of EYFP and ECFP into the ROSA26 locus. *BMC Dev. Biol.* 1:4. doi: 10.1186/1471-213x-1-4

Stenmark, H. (2009). Rab GTPases as coordinators of vesicle traffic. *Nat. Rev. Mol. Cell Biol.* 10, 513–525. doi: 10.1038/nrm2728

Stephen, L. A., Johnson, E. J., Davis, G. M., McTeir, L., Pinkham, J., Jaberi, N., et al. (2014). The chicken left right organizer has nonmotile cilia which are lost in a stage-dependent manner in the talpid3 ciliopathy. *Genesis* 52, 600–613. doi: 10.1002/dvg.22775

Stephen, L. A., Tawamie, H., Davis, G. M., Tebbe, L., Nurnberg, P., Nurnberg, G., et al. (2015). TALPID3 controls centrosome and cell polarity and the human ortholog KIAA0586 is mutated in Joubert syndrome (JBTS23). *Elife* 4:e08077. doi: 10.7554/eLife.08077

Sung, C.-H., and Leroux, M. R. (2013). The roles of evolutionarily conserved functional modules in cilia-related trafficking. *Nat. Cell Biol.* 15, 1387–1397. doi: 10.1038/ncb2888

Tennyson, V. M., Payette, R. F., Rothman, T. P., and Gershon, M. D. (1990). Distribution of hyaluronic acid and chondroitin sulfate proteoglycans in the presumptive aganglionic terminal bowel of ls/ls fetal mice: an ultrastructural analysis. *J. Comp. Neurol.* 291, 345–362. doi: 10.1002/cne.902910303

Thiagarajah, J. R., Yildiz, H., Carlson, T., Thomas, A. R., Steiger, C., Pieretti, A., et al. (2014). Altered goblet cell differentiation and surface mucus properties in Hirschsprung disease. *PLoS One* 9:e99944. doi: 10.1371/journal.pone.0099944

Thomas, P. S., Kim, J., Nunez, S., Glogauer, M., and Kaartinen, V. (2010). Neural crest cell-specific deletion of Rac1 results in defective cell–matrix interactions and severe craniofacial and cardiovascular malformations. *Dev. Biol.* 340, 613–625. doi: 10.1016/j.ydbio.2010.02.021

Tsai, J. J., Hsu, W. B., Liu, J. H., Chang, C. W., and Tang, T. K. (2019). CEP120 interacts with C2CD3 and Talpid3 and is required for centriole appendage assembly and ciliogenesis. *Sci. Rep.* 9:6037. doi: 10.1038/s41598-019-42577-0

van den Brink, G. R. (2007). Hedgehog signaling in development and homeostasis of the gastrointestinal tract. *Physiol. Rev.* 87, 1343–1375. doi: 10.1152/physrev.00054.2006

Villumsen, B. H., Danielsen, J. R., Povlsen, L., Sylvestersen, K. B., Merdes, A., Beli, P., et al. (2013). A new cellular stress response that triggers centriolar satellite reorganization and ciliogenesis. *EMBO J.* 32, 3029–3040. doi: 10.1038/emboj.2013.223

Waldo, K. L., Hutson, M. R., Stadt, H. A., Zdanowicz, M., Zdanowicz, J., and Kirby, M. L. (2005). Cardiac neural crest is necessary for normal addition of the myocardium to the arterial pole from the secondary heart field. *Dev. Biol.* 281, 66–77. doi: 10.1016/j.ydbio.2005.02.011

Wallace, A. S., and Burns, A. J. (2005). Development of the enteric nervous system, smooth muscle and interstitial cells of Cajal in the human gastrointestinal tract. *Cell Tissue Res.* 319, 367–382. doi: 10.1007/s00441-004-1023-2

Wang, L., Lee, K., Malonis, R., Sanchez, I., and Dynlacht, B. D. (2016). Tethering of an E3 ligase by PCM1 regulates the abundance of centrosomal KIAA0586/Talpid3 and promotes ciliogenesis. *Elife* 5:e12950. doi: 10.7554/eLife.12950

Willaredt, M. A., Hasenpusch-Theil, K., Gardner, H. A., Kitanovic, I., Hirschfeld-Warneken, V. C., Gojak, C. P., et al. (2008). A crucial role for primary cilia in cortical morphogenesis. *J. Neurosci.* 28, 12887–12900. doi: 10.1523/JNEUROSCI.2084-08.2008

Wu, C., Yang, M., Li, J., Wang, C., Cao, T., Tao, K., et al. (2014). Talpid3-binding centrosomal protein Cep120 is required for centriole duplication and proliferation of cerebellar granule neuron progenitors. *PLoS One* 9:e107943. doi: 10.1371/journal.pone.0107943

Yan, H., Chen, C., Chen, H., Hong, H., Huang, Y., Ling, K., et al. (2020). TALPID3 and ANKRD26 selectively orchestrate FBF1 localization and cilia gating. *Nat. Commun.* 11:2196. doi: 10.1038/s41467-020-16042-w

Yin, Y., Bangs, F., Paton, I. R., Prescott, A., James, J., Davey, M. G., et al. (2009). The Talpid3 gene (KIAA0586) encodes a centrosomal protein that is essential for primary cilia formation. *Development* 136, 655–664. doi: 10.1242/dev.028464

Zorn, A. M., and Wells, J. M. (2009). Vertebrate Endoderm Development and Organ Formation. *Annu. Rev. Cell Dev. Biol.* 25, 221–251. doi: 10.1146/annurev.cellbio.042308.113344

Conflict of Interest: AB is currently a full time employee of Takeda Pharmaceuticals International Inc.

The remaining authors declare that the research was conducted in the absence of any commercial or financial relationships that could be construed as a potential conflict of interest.

Publisher's Note: All claims expressed in this article are solely those of the authors and do not necessarily represent those of their affiliated organizations, or those of the publisher, the editors and the reviewers. Any product that may be evaluated in this article, or claim that may be made by its manufacturer, is not guaranteed or endorsed by the publisher.